



Experimental evaluation of automatically-generated behaviors for USV operations



Ivan R. Bertaska ^{a,*}, Brual Shah ^b, Karl von Ellenrieder ^a, Petr Švec ^b, Wilhelm Klinger ^a, Armando J. Sinisterra ^a, Manhar Dhanak ^a, Satyandra K. Gupta ^b

^a Department of Ocean & Mechanical Engineering, Florida Atlantic University, 101N. Beach Road, Dania Beach, FL 33004, United States

^b Maryland Robotics Center, Department of Mechanical Engineering, University of Maryland, College Park, MD 20742, United States

ARTICLE INFO

Article history:

Received 15 November 2014

Accepted 5 July 2015

Available online 6 August 2015

Keywords:

Marine vehicles

Unmanned surface vehicles

COLREGs

Guidance, navigation and control

Lattice-based trajectory planning

Nonlinear control

ABSTRACT

The performance of four automatically-generated path planning behaviors is evaluated through field-testing. Experiments were conducted using a model-referenced trajectory planner, which was implemented on unmanned surface vehicles (USVs) of different size, thrust, and maneuverability characteristics. The planner combines a local search based on the Velocity Obstacles (VO) concept with a global, lattice-based search for a dynamically feasible trajectory (determined using models of the nonlinear dynamics, nonholonomic constraints, and low-level control of each system). Multiple low-level USV heading and speed controllers, varying in complexity from proportional control to nonlinear backstepping control, were tested with the planner. High planning performance is achieved by searching within a resolution-adaptive space of the USV's candidate motion goals. Sampling is constrained to ensure that the International Regulations for the Prevention of Collisions at Sea (COLREGs) are followed. Prior to on-water implementation, the system was fine-tuned in simulation. Four automatically-generated USV behaviors were demonstrated in on-water tests within a complex, static obstacle field: 1) Approach (USV approaches a fixed target); 2) Follow (USV approaches a moving target); 3) Single COLREGs-Compliant Crossing (USV approaches a fixed target while avoiding another vessel); and 4) Multiple COLREGs-Compliant Crossings (USV approaches a fixed target while avoiding an interference vessel multiple times).

© 2015 Elsevier Ltd. All rights reserved.

1. Introduction

Today, unmanned surface vehicles (USVs) are not truly capable of persistent autonomy due to the wide variety of tasks they must perform and the complexity of their operating environments. The more tractable command and control architectures of unmanned vehicles tends to be multilayered, where decision-making, sensing, and actuation are separated so that the number of internal states of the system can be kept to a minimum (Bingham et al., 2011; Gat, 1993, 1998; Ridao et al., 1999). Here, we focus on the interplay between two layers of such an architecture, a higher-level trajectory planner and a low-level controller. Contemporary USV trajectory planners generally rely on waypoint navigation and scripted operations for trajectory control. In order for USVs to operate in complex environments, a combination of advanced deliberative and reactive planning is necessary. This may be achieved through a realized set of "automatically-generated" behaviors, which enhance the planner so that it considers different classes of situations in pre-programmed

ways. Here, we refer to the generation of trajectories by the planner as "the automatic generation of behaviors," since the interchange between the high-level planner and the low-level controller is not dictated by a human operator.

In practice, most USVs are underactuated, and their motion is restricted by nonholonomic kinematic constraints and the limited control authority of real actuators. To ensure that a USV can execute a planned trajectory with minimal error, and thus help to guarantee collision-free operation, the trajectories generated by the planner should account for the inherent limitations of the vehicle's dynamic response. Here, this is accomplished by first using the dynamic response model of a controlled USV (obtained through a combination of physics-based modeling, system identification testing, and on-water validation) to learn and tune behaviors within a virtual simulation environment (Švec and Gupta, 2012; Thukar et al., 2012). The tuned planner is then implemented on the USV, where the dynamic response model of the controlled USV is used to generate dynamically feasible trajectories in real-time in response to navigational sensor inputs (Bertaska et al., 2013; Švec et al., 2014a).

Also of significant interest is the capability for USVs to navigate along trajectories that abide by common waterway laws, without explicit supervision (Švec et al. 2013, 2014a) for which model

* Correspondence to: Florida Atlantic University, 101 N. Beach Rd., Dania Beach, FL 33004-3023 USA. Tel.: +1 954 683 4046.

E-mail address: ibertask@fau.edu (I.R. Bertaska).

validated trajectory generation is essential. Several approaches have been proposed, but few have been validated with full-sized, multi-vehicle experiments in the presence of static obstacles and boundaries (Benjamin et al., 2006; Kuwata et al., 2014). Very recently, techniques have been developed that aim to address this challenge (Bareiss and van den Berg, 2013; van den Berg et al., 2011, 2012; Wilkie et al., 2009). However, these techniques are based on simplifying assumptions about the vehicle's dynamics, do not have the capability to utilize advanced low-level control and rich sets of control actions in planning, or do not consider constraints on control inputs. Linearization of the vehicle model leads to restricted performance around a nominal speed and precludes the possibility of using a broad range of the vehicle's dynamics.

In this paper, work on the modeling and development of control systems is described that progresses from traditional proportional controls to nonlinear controls, in support of developing matching planning algorithms that take into account the vehicle dynamics and controller performance. The automatically-generated behaviors provide a deliberative/reactive method that allows a USV to interact with objects in its environment. The high-level planner reacts to changes in the environment by modifying the trajectory sent to the low-level control system. The vehicle then follows suit, reacting to that change. First, a three degree of freedom (3 DOF) dynamic model of each vehicle is created, following Fossen (1994), that includes cross-coupled terms in added mass and drag parameter matrices. A modified P-controller is developed to manage vehicle heading, which is then extended to also control surge speed. Successful field trials of these traditional controllers are presented in conjunction with a Line-of-Sight (LOS) maneuvering system to navigate the vehicle through a series of set-point commands. The same LOS system is later augmented with a nonlinear, backstepping controller similar to that proposed in Liao et al. (2010). However, here centripetal and nonlinear drag terms are taken into account so that the vehicle can follow a path with a larger variation in speed, ultimately resulting in improved performance in maneuvering under more dynamic requirements – good maneuvering is important for effective collision avoidance.

The autonomous navigation of USVs is primarily dependent on their capability to avoid static obstacle regions as well as operate in civilian traffic. The planning algorithm developed in this work is capable of avoiding static as well as dynamic obstacles (i.e., marine vessels) and complying with COLREGs rules standardized by the International Maritime Organization (IMO) (Commandant, 1999). The planner tightly combines the USV's dynamics and low-level controller in the planning phase to enable the vehicle to operate in complex dynamic environments (e.g., harbors). A 3 DOF simulation model of the USV's dynamics and control is incorporated into trajectory planning to estimate trajectories the USV will execute for several candidate control inputs and select the one with the lowest cost. The model is used to design a discrete set of the USV's control variables (i.e. surge speed, and heading), which is used for the computation of global trajectories as well as local maneuvers. Thus, the same planning algorithms can be used for vehicles with different dynamics and low-level control. Implementations of the velocity obstacle approach commonly use kinematic models of the vehicle, which are prone to the generation of trajectories that are not dynamically feasible. When a vessel changes its dynamic operating regime (e.g. from running at displacement hull speeds to planing hull speeds), or a vehicle is operating near a limit of its dynamic range (such as in high winds or currents), the need for a planner that can generate dynamically feasible trajectories becomes critical. The developed planners are made computationally efficient through adaptively changing the resolution of the search space and performing focused sampling in areas with promising trajectories towards the goal. This allows the USV to compute trajectories in real-time and have a higher replanning rate, in general. One side benefit of this approach is that the high replanning rate helps to

mitigate the effects of environmental disturbances. Different versions of the planner were developed with increasing complexity to operate in static, less congested scenarios as well as complex harbor scenarios with "other moving traffic" (OMT) vessels.

The automatically-generated behaviors provide a deliberative/reactive approach that allows a USV to interact with objects in its environment, including other autonomous vehicles, obstacles, and boat traffic. The high-level planner reacts by modifying the trajectory sent to the low-level control system. For example, in a static environment, i.e. with only static obstacles, a deliberative, global planner is used to find an optimized trajectory to reach a certain state, in this case, a desired pose (x_d, y_d, ψ_d) while avoiding obstacles. When a dynamic feature is encountered, i.e. boat traffic, a local planner takes over and automatically generates a new trajectory to guide the vehicle in compliance with certain rule sets. These include the COLREGs crossing rules, as well as collision avoidance procedures.

The controllers and trajectory planners developed through this work have been repeatedly tested via physical experiments on various USV platforms in the presence of environmental disturbances. The experiments demonstrate a variety of tasks that were successfully completed using the developed control and planning approach. A four-step effort in validating automatically-generated behaviors for USV operations in a constrained environment is utilized:

1. An "Approach" behavior is tested where an interceptor USV follows a path to a static target within a static obstacle field.
2. A "Follow" behavior is generated, which features tracking of a target USV within a similar static obstacle field by the interceptor USV, maintaining a set distance from the target.
3. COLREGs-compliant crossing situations are tested in which the interceptor USV navigates a crowded waterway with several static obstacles towards a static target point, but along the way, the interceptor USV encounters an interference vessel and must cross its trajectory in compliance with COLREGs. Head-on, crossing from starboard, and overtaking situations were considered and evaluated.
4. A combination of the first and third scenario is expanded upon by using multiple COLREGs crossing situations in a constrained harbor-like region. Successful COLREGs avoidance with one vessel may lead to a collision with other vessels or static obstacles in the path of the USV. Planner capabilities were stressed by experimentally mimicking multiple crossings using a single human-operated vehicle.

A background to the problem is provided in Section 2; a description of the 3 DOF maneuvering model used for the USVs is given in Section 3; the control laws and planning algorithms used for each test are presented in Section 4; the experimental set-up and procedures utilized in the experiments, together with the software architecture of the low-level controller and high-level planner are described in Section 5; and the results of each experiment are presented in Section 6. Finally, in Section 7, some concluding remarks are given concerning the implications of the results.

2. Related work

Recent work in control systems for underactuated marine vehicles has proposed nonlinear set-point control and trajectory tracking (Aguiar and Hespanha, 2003; Aguiar et al., 2003; Alvarez et al., 2013; Ashrafiou et al., 2008, 2010; Do, 2010; Do and Pan, 2003; Mahini and Ashrafiou, 2012; Sonnenburg and Woolsey, 2013). However, few of these control systems have been tested on physical USV platforms (Ashrafiou et al., 2010). Instead, the focus has been on the development of nonlinear control methods, typically with simplifying assumptions about vehicle dynamics.

Implementation has largely been limited to small scale experiments and simulation. A planar, 3 DOF model is used with control forces acting exclusively in the surge and yaw directions. Pettersen and Egeland (1996) showed that underactuated vehicles without gravitational and buoyant forces cannot be asymptotically stabilized by continuous, time invariant state feedback. However, control laws can be derived that are accessible at all points and remain locally controllable (Ashrafiou, et al., 2010). Recent examples of such control laws include sliding-mode target and trajectory tracking (Ashrafiou, et al., 2008; Mahini and Ashrafiou, 2012) as well as Lyapunov-based backstepping techniques (Aguiar and Hespanha, 2003; Aguiar et al., 2003) that were validated on a model hovercraft. These controllers assumed diagonalized parameter matrices, which may not fully capture the behavior of the physical system. Do and Pan (2003) extended the work with backstepping controllers to include non-diagonal parameter matrices using a change of coordinates to produce a system in strict feedback form. This allows for the application of recursive backstepping similar to that proposed in Khalil (2002). However, results for the controllers proposed in this manner were restricted to simulations (Do, 2010). Contemporary physical experiments have featured target following capabilities using a yaw controller based on Lyapunov methods, as in Bibuli et al. (2012), but employed a modified proportional-integral controller to manage surge speed. Sonnenburg and Wooley (2013) proposed a proportional derivative controller, as well as a backstepping technique with a speed scheduled vehicle model. The authors derived the vehicle maneuvering characteristics using several versions of the Nomoto Steering Model, which simplified the yaw angular acceleration to be dependent on rudder deflection and yaw velocity, and did not directly take into account the effect of sway velocity at all speeds. Furthermore, the centripetal term was neglected in construction of the forward speed model of their vehicle, which becomes important for a vessel operating at low speeds in the presence of exogenous disturbances.

A recent review of several different approaches for the implementation of COLREGs-compliant path planning for USVs can be found in Campbell et al. (2012). These methodologies include map-based techniques (Gadre et al., 2012; Stilwell et al., 2011) and local velocity obstacle (VO) approaches (Kuwata et al., 2014), sometimes combined with deliberative planners to allow global guidance. As pointed out in Kuwata et al. (2014), map-based methods do not scale well to traffic with multiple boats that have multiple COLREGs requirements and tend to be difficult to implement on physical

platforms with real-time computational requirements. Important advantages of the VO approach are that it can be used to check the collisions of vehicles following arbitrary trajectories, is fast to compute, and extends well to high speed operations with short reaction times. The works summarized here (Bertaska et al., 2013; Švec et al., 2014a) are based on the generalized velocity obstacle approach (GVO) (Willie et al., 2009) for COLREGs-compliant trajectory planning that considers the USV's nonlinear dynamics and low-level control. The VO approach typically works well for fully actuated systems capable of maneuvering in any specified direction, but may not adequately capture the motions of nonholonomic systems. Accordingly, the dynamics and instantaneous state of a USV may impose constraints that affect its ability to maneuver, such as stopping distance or minimum turning radius. Use of the planner developed here helps to ensure that, in addition to satisfying COLREGs and motion goals, the trajectories generated by the planner are dynamically feasible (Švec et al., 2013). While incorporation of the vessel dynamics may incur additional computational cost, the framework can be implemented with any low-level controller and may be sped up by dynamically adapting the resolution of the state space lattice used for a trajectory search (Švec et al. 2014a, 2014b).

3. USV maneuvering model

The USVs modeled herein are twin-hulled vehicles, which are steered using differential thrust. A 3 DOF model of each USV is constructed using established techniques (Fossen, 1994; Klinger et al., 2013; Marquardt et al., 2014). Each model is restricted to 3 DOF planar motion (surge, sway, and yaw) and includes coupled sway-yaw hydrodynamic terms and a nonlinear centripetal matrix, which couples the three system states in a nonlinear manner. Speeds are limited to the displacement and lower semi-planing regions of operation. The other DOF, heave velocity, pitch rate, and roll rate, are neglected as they only tend to become significant in the upper semi-planing and planing hull speeds. The maneuvering models take into account control forces, the mass and the added mass matrices, a nonlinear drag-damping matrix, and a nonlinear centripetal matrix. Control forces from the differential thrust are solved using the control allocation described below. All values for the parameters presented in this section were identified using a combination of empirical formulas and system identification tests as described in Alvarez et al. (2013) and Klinger et al., Submitted for publication. The 3 DOF dynamic model is presented in Fossen (1994) in vector form as:

$$\mathbf{M}\mathbf{v} + \mathbf{C}(\mathbf{v})\mathbf{v} + \mathbf{D}(\mathbf{v})\mathbf{v} = \boldsymbol{\tau}. \quad (1)$$

where the system states are given as $\mathbf{v} = [u, v, r]^T$, denoting the surge velocity, sway velocity and yaw rate of the vehicle, respectively, in the body-fixed coordinate system (Fig. 1). The origin of the body-fixed frame is taken to be the center of gravity of the USV. The control forces $\boldsymbol{\tau}$ are also represented in the body-fixed reference frame as $\boldsymbol{\tau} = [X, Y, N]^T$, where each element is the summation of the induced forces in its respective direction. This includes the control forces, as well as any environmental forces that may act on the vehicle (e.g., wind, current, waves). The mass, hydrodynamic, and centripetal coefficient terms, \mathbf{M} , $\mathbf{D}(\mathbf{v})$, and $\mathbf{C}(\mathbf{v})$ are 3×3 matrices as given by Table 1. \mathbf{M} is a combination of the diagonal mass and inertia matrix and added mass terms, $\mathbf{M} = \mathbf{M}_{RB} + \mathbf{M}_A$. $\mathbf{D}(\mathbf{v})$ is the summation of the linear and nonlinear damping matrix corresponding to the drag on the vehicle as $\mathbf{D}(\mathbf{v}) = \mathbf{D}_L + \mathbf{D}_n(\mathbf{v})$. The centripetal term $\mathbf{C}(\mathbf{v})$ is also a summation of the rigid body and added mass terms as $\mathbf{C}(\mathbf{v}) = \mathbf{C}_{RB}(\mathbf{v}) + \mathbf{C}_A(\mathbf{v})$. The values within the matrices in Table 1 are hydrodynamic coefficients from a linearization of the Taylor series expansion of the forces acting on a vehicle. The SNAME 1950 notation is used where subscripted terms are states that relate to the forces in

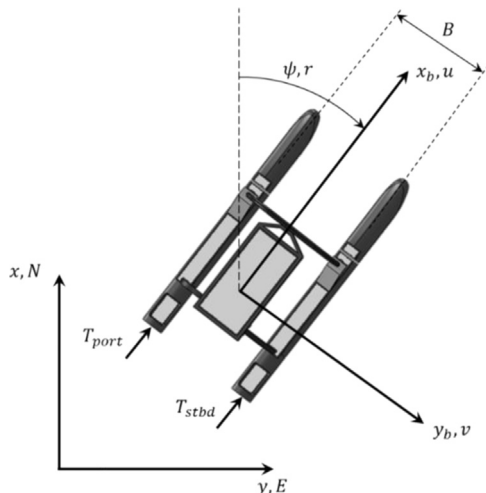


Fig. 1. Definition of the NED and body-fixed coordinate systems used to develop USV planar motion models. The origin of the body-fixed coordinate system is taken as the center of gravity of the vehicle.

Table 1
Mass parameter, drag parameter, and centripetal matrices for 3 DOF system.

$$\begin{aligned}
 \mathbf{M}_{RB} &= \begin{bmatrix} m & 0 & -my_G \\ 0 & m & mx_G \\ -my_G & mx_G & I_z \end{bmatrix} \\
 \mathbf{D}_L &= - \begin{bmatrix} X_u & 0 & 0 \\ 0 & Y_v & Y_r \\ 0 & N_v & N_r \end{bmatrix} \\
 \mathbf{C}_{RB} &= \begin{bmatrix} 0 & 0 & -m(x_G r + v) \\ 0 & 0 & -m(y_G r - u) \\ m(x_G r + v) & m(y_G r - u) & 0 \end{bmatrix} \\
 \mathbf{M}_A &= \begin{bmatrix} -X_{\dot{u}} & 0 & 0 \\ 0 & -Y_{\dot{v}} & -Y_{\dot{r}} \\ 0 & -N_{\dot{v}} & -N_{\dot{r}} \end{bmatrix} \\
 \mathbf{D}_n &= - \begin{bmatrix} X_{|u|u|u|} & 0 & 0 \\ 0 & Y_{|v|v|v|} + Y_{|r|r|r|} & Y_{|v|r|r|} + Y_{|r|r|r|} \\ 0 & N_{|v|v|r|} + N_{|r|r|r|} & N_{|v|r|r|} + N_{|r|r|r|} \end{bmatrix} \\
 \mathbf{C}_A &= \begin{bmatrix} 0 & 0 & Y_v v + \frac{Y_r + N_u}{2} r \\ 0 & 0 & -X_u u \\ -(Y_v v + \frac{Y_r + N_u}{2} r) & X_u u & 0 \end{bmatrix}.
 \end{aligned}$$

uppercase terms, e.g. Y_r is the drag coefficient in the Y direction due to angular velocity in the direction of r (Fossen, 1994).

The dynamic model of the vehicle is derived in the body-fixed coordinate system. To transfer these equations to the North-East-Down (NED) geographic coordinate system (Fig. 1), a transformation matrix is used. The states from the body-fixed model $\mathbf{v} = [u, v, r]^T$ are converted into their geographic equivalents, $\dot{\eta} = [\dot{x}, \dot{y}, \dot{\psi}]^T$, where \dot{x} is the velocity in the North direction, \dot{y} is the velocity in East, and $\dot{\psi}$ is z-axis angular velocity, which in this case is directly related to the yaw rate as $\dot{\psi} = r$. The transformation from body-fixed coordinates to geographic coordinates is:

$$\begin{bmatrix} \dot{x} \\ \dot{y} \\ \dot{\psi} \end{bmatrix} = \begin{bmatrix} \cos \psi & -\sin \psi & 0 \\ \sin \psi & \cos \psi & 0 \\ 0 & 0 & 1 \end{bmatrix} \begin{bmatrix} u \\ v \\ r \end{bmatrix}. \quad (2)$$

Each USV uses either dual propellers or dual waterjets for propulsion (see Section 5.1). The relationship between thrust developed and the commanded waterjet impeller/propeller speed in revolutions per minute (RPM) was assumed to be approximately linear in the operating range of the experiments conducted. The thrust is approximated as $T = T_{max} \text{RPM}/\text{RPM}_{max}$, where T_{max} is the maximum thrust produced by each propulsor and RPM_{max} is the maximum waterjet impeller/propeller speed. The resultant allocation for the control force τ is:

$$\tau = \begin{bmatrix} (T_{port} + T_{stbd}) \\ 0 \\ (T_{port} - T_{stbd})B/2 \end{bmatrix}, \quad (3)$$

where T_{port} and T_{stbd} are the port and starboard thrust, respectively, and B is the center-line to center-line hull separation, as shown in Fig. 1. The null term in the control force vector is indicative of the fact that each USV is underactuated, since it cannot produce a force in the sway direction. This becomes significant when deriving control laws for the vehicle, as is demonstrated in Section 4.

4. Implementation of the guidance, navigation and control systems on USV platforms

4.1. Control

Three sets of control algorithms were derived for the experiments, increasing in complexity. The first was a proportional control law that regulated the vehicle heading error to a set-point with open loop control of vehicle speed. This is suitable for the “Approach” experiment. However, for the “Following” experiment, the USV must utilize a sizeable breadth of its dynamic range to track a target over a range of speeds. Accordingly, two P-controllers were then developed to control vehicle yaw and surge speed. Ultimately, these two control laws forced a linearized model of the vehicles and were subject to errors due to nonlinear effects. For the experiments comprising

COLREGs-compliant crossings, the USV would be in close proximity with another moving vessel, necessitating accurate speed tracking over the vehicle's full dynamic range. To overcome this issue and improve performance, a set-point backstepping control law was derived and implemented following the approach presented in Liao et al. (2010). The development and validation of these control laws is presented in Bertaska et al. (2013), Klinger et al. (2013) and Klinger et al. (Submitted for publication), but is excluded here for brevity.

4.1.1. Experiment 1, “Approach” control system

Due to differential steering, the vehicle heading controller differs from those that utilize rudder steering systems as in Fossen (1994) and Sonnenburg and Woolsey (2013). Differential steering imposes a moment about the vehicle that causes it to turn. There are distinct advantages to this type of system; primarily, the turning radius for the vehicle is substantially reduced, as well as the additional capability to steer without the requirement of a forward speed. With this configuration, the controller manages vehicle direction by two separate proportional control laws. Each of these controllers focuses on a single motor. Owing to the yaw NED convention, the port controller would have a positive slope, while the starboard controller would have a negative slope (Bertaska et al., 2013). The error for this system was taken to be the difference between the actual heading and the heading estimate, as $e = \psi_d - \psi$, wrapped around the 360° mark. A tolerance region where the magnitude of the error was less than a threshold, θ , of $\theta = 5^\circ$ was implemented to allow a small fluctuation in heading before being corrected by the P-controller. For the experiment that utilized this controller, vehicle speed was not a factor – surge velocity was left as an open-loop control. An offset denoting a percentage of the full-scale motor command was used to provide a forward speed to the vehicle. The control law was biased by this value as is shown in Fig. 2. Ideally, when the vehicle was operating in the tolerance region, it would follow a straight course at the given motor command. The motor bias was hard-set before the start of the mission, and did not vary during operation. It is important to note that the maneuverability of the USV was inversely related to this motor bias, i.e. a higher motor bias would effectively limit the amount of torque left for turning. Hence, a lower bias would result in less forward thrust, but more potential steering torque, leading to greater maneuverability. Note that two of the three experimental USV platforms (see Section 5) are propelled by waterjets. These vessels do not produce reverse thrust (reversing buckets were not used), so negative motor commands to these vessels were thresholded to zero.

A LOS maneuvering system was used to control USV position and transition between waypoints in a trajectory as in Fossen (2002). This system used the vehicle's current position and desired position to determine a desired heading, ψ_d . This was calculated using $\psi_d = \tan^{-1}[(x_i - x)/(y_i - y)]$, where x and y are coordinates in NED, and the i subscript denotes the i th waypoint in the trajectory and the current destination of the USV. An argument

against such a system would be that for more distant waypoints large cross track errors could become prevalent due to wave and wind disturbances (Fossen, 2002). This problem was circumvented by spacing each waypoint in the trajectory sufficiently close to the current position of the vehicle so that any off-course perturbations were minimal.

4.1.2. "Follow" (Experiment 2) and "COLREGs-compliant crossings" (Experiment 3) control system

A combination of P-controllers was devised to simultaneously control vehicle heading and surge velocity. The differential thrust configuration of each USV requires its propulsion units to develop forward speed while simultaneously turning the vehicle. Thus, two controllers were developed around the feedback from the vehicle heading, ψ , and surge velocity, u . A negative feedback loop was used to maintain that speed in the presence of perturbations. A depiction of this control system is found in the block diagram in Fig. 3.

The heading controller functions similarly to the one described in Section 4.1.1, with the exception that the motor offset is varied to maintain a desired surge speed. This causes the control law to be shifted up or down on the motor command axis (Fig. 4). Careful tuning of the gains causes the vehicle to respond to either heading or speed errors more sharply. For these tests, maneuverability was chosen over speed capabilities, and gains were set to control the heading error first, although both errors are regulated (Alvarez et al., 2013). As mentioned in Section 4.1.1 above, negative motor commands to the USV platforms propelled by waterjets were thresholded to zero.

4.1.3. Experiment 4 "Approach with multiple COLREGs-compliant crossings" control system

A nonlinear, set-point controller was derived with a basis on Liao et al. (2010) to regulate vehicle heading and surge velocity. Nonlinear controllers are derived from the nonlinear vehicle model, and thus, outperform linear controllers over a wider range of speeds. In addition to this performance boost, the nonlinear set-point controller derived here allows a user-set resistance in acceleration. Hence, the rise time and work from the motor can be traded off according to battery capacity and controller performance.

In deriving the controller, the cross terms associated with the added mass and damping matrices are neglected, i.e. the mass and drag matrices become diagonal. However, the centripetal matrix

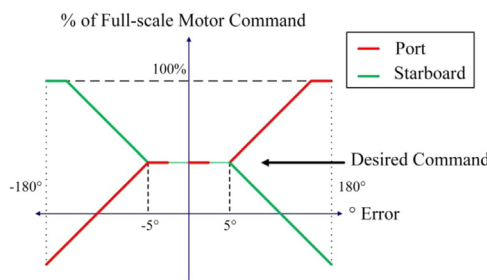


Fig. 2. Proportional heading controller – “Approach” (Experiment 1).

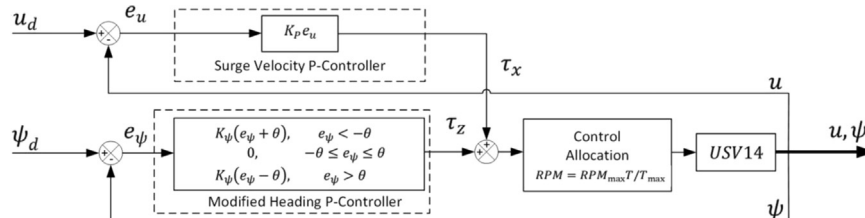


Fig. 3. Block diagram of the speed and heading controller. Gains K_ψ and K_u were selected based on performance. Surge speed error and heading error are denoted as e_u and e_ψ , respectively. θ is the heading tolerance (see Section 4.1.1).

remains, and the nonlinearities created by it are backstepped out through the controller derivation. Under these assumptions, the vehicle model reduces to:

$$\dot{u} = \frac{(m - Y_v)v_r + X_u u + X}{m - X_u}, \quad (4)$$

$$\dot{v} = \frac{(m - X_u)u_r + Y_v v}{m - Y_v}, \quad (5)$$

$$\dot{r} = \frac{(-X_u + Y_v)uv + N_r r + N}{I_z - N_f}, \quad (6)$$

$$\dot{\psi} = r \quad (7)$$

As the system is underactuated in the sway direction, the control problem reduces to control of the surge and yaw subsystems. The control force X can be determined from the surge subsystem equation

$$X = -(m - Y_v)v_r - X_u u + (m - X_u)\dot{u}. \quad (8)$$

A backstepping variable z_u is chosen as $z_u = u - u_d$, where u_d is the desired surge velocity. Taking the derivative of the backstepping variable and substituting the surge acceleration produces

$$\dot{z}_u = \frac{(m - Y_v)v_r + X_u u + X}{m - X_u} - \dot{u}_d \quad (9)$$

To cancel nonlinearities, the control force in the surge direction can be defined according to feedback linearization as:

$$X = (m - X_u)[\dot{u}_d - k_{u,1}z_u] - [(m - Y_v)v_r + X_u u]. \quad (10)$$

A stability analysis with the candidate Lyapunov function $V_u = (1/2)z_u^2$ produces a negative definite function for $k_{u,1} > 0$. As this is a set-point controller, a desired surge acceleration is not given, and must be constructed dependent on the maximum acceleration of the vehicle $\dot{u}_{a,max}$, maximum velocity during turns $u_{d,yaw}$, and the error in heading ψ_e :

$$\dot{u}_d = \dot{u}_{a,max} \tan h \left[\frac{k_{a,max}(u_{d,ref} - u)}{\dot{u}_{a,max}} \right]. \quad (11)$$

Both $\dot{u}_{a,max}$ and $k_{a,max}$ can be tuned to improve vehicle performance. This leaves the reference surge velocity $u_{d,ref}$ to be defined according to the minimum function between the surge velocity

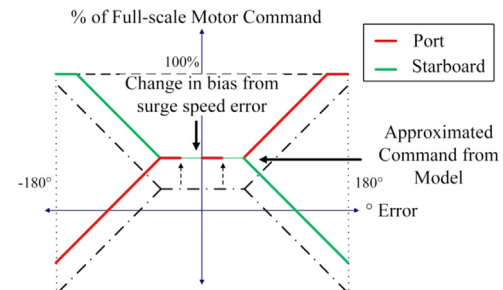


Fig. 4. Proportional surge speed and heading control motor commands – “Follow” (Experiment 2) and COLREGs-compliant crossings (Experiment 3).

while turning and the desired surge velocity.

$$u_{d,\text{ref}} = \min \left\{ \left[u_{d,\text{yaw}} + (u_d - u_{d,\text{yaw}}) e^{-5.73|\psi_e|} \right], u_d \right\}. \quad (12)$$

Setting the desired surge acceleration in this manner forces the controller to give priority to the heading error, while regulating the surge velocity error later. Because of the differential thrust configuration of each USV, this leads to a more maneuverable vehicle, while allowing full power from the motors during transit, and dropping the speed to $u_{d,\text{yaw}}$ during corners.

Input state linearization (Slotine and Li, 1991) can be used to find a nonlinear feedback control law for the yaw subsystem. Let ξ be a linearizing control, related to the torque input N as

$$N = (I_z - N_r)\xi - (-X_{\dot{u}} + Y_{\dot{v}})uv - N_r, \quad (13)$$

using this in (6) gives $\dot{r} = \ddot{\psi} = \xi$. If the heading tracking error is defined as $e_{\psi} = (\psi - \psi_d)$, where ψ_d is the desired heading angle, and an input of the form $\xi = \ddot{\psi} = \ddot{\psi}_d - k_1 e_{\psi} - k_2 \dot{e}_{\psi}$ is selected, the error dynamics will be:

$$\ddot{e}_{\psi} + k_2 \dot{e}_{\psi} + k_1 e_{\psi} = 0, \quad (14)$$

which is exponentially stable for control gains $k_1 > 0$ and $k_2 > 0$. Although developed in a different way, the form of this solution is functionally equivalent to that developed for the yaw subsystem in Liao et al. (2010). Only the desired heading ψ_d (and not also $\dot{\psi}_d$ and $\ddot{\psi}_d$) is provided by the LOS navigation system. This results in the control law:

$$N = (I_z - N_r)(-k_1 e_{\psi} - k_2 r) - (-X_{\dot{u}} + Y_{\dot{v}})uv - N_r. \quad (15)$$

Combining both the surge speed and heading controllers results in a system state (u, r, ψ) that is bounded and globally uniformly asymptotically convergent to $(u_d, 0, \psi_d)$ when $t \rightarrow \infty$, and well-defined and bounded for all $t > 0$. Modifications of the resultant control law to handle actuator saturation are described in Klinger et al. (Submitted for publication).

4.2. Trajectory planning

The trajectory planning for the presented problem can be performed by several classes of algorithms such as reactive or local planning methods (Fiorini and Shiller, 1998; Fox et al., 1997; Fraichard and Asama, 2004; Lee et al., 2004), deliberative or global planning (Hart et al., 1968; Likhachev et al., 2005; Pivtoraiko et al., 2009) and coupled trajectory planning using global and local planning methods (Howard et al., 2008; Sgorbissa and Zaccaria, 2012; Stachniss and Burgard, 2002). The local planning methods will not work satisfactorily for scenarios having local minima. In addition, the follow behavior requires the USV to robustly maintain the same heading as that of the target vehicle, this is difficult to achieve using local planning methods. The global planning methods solve the problem of local minima in an environment with static obstacles, but they do not perform well within an environment with dynamic obstacles (OMT vessels). Thus, we have implemented a combined approach of using global and local planning methods. The global planners compute trajectories that avoid static obstacles in the environment, and the local planners are used reactively to avoid OMT vessels in a COLREGs-compliant manner.

We have developed a tightly integrated model-predictive trajectory planning and tracking algorithm for avoiding static obstacle regions as well as dynamic OMT vessels. The algorithm developed in this research combines global and local trajectory planners and integrates them with low-level feedback controllers to ensure safe, efficient, and COLREGs-compliant operation of the USV in a highly cluttered environment. The global lattice-based trajectory planner (see Section 4.2.2) is primarily used for computation of collision-free, dynamically feasible, global trajectories for the USV. On the other hand, the local velocity obstacle-based planner is used for high fidelity, COLREGs-compliant avoidance of dynamic OMT

vessels. The switching between the global and local trajectory planners is determined by the user-defined parameters called the time t_{CPA} to the closest point of approach (CPA) and the distance d_{CPA} between the USV and surrounding OMT vessels at the CPA (Švec et al., 2013).

4.2.1. Definitions

This subsection formally defines the notation used to describe the global and local trajectory planners. Let $X = X_{\eta} \times X_v \times T$ be the continuous state space in which each state $\mathbf{x} = [\eta^T, v^T, t]^T$ consists of the USV's position $\eta = [x, y, \psi]^T \in X_{\eta} \subset \mathbb{R}^2 \times \mathbb{S}^1$, velocity $v = [u, v, r]^T \in X_v \subset \mathbb{R}^3$, and time t . The USV's position consists of x and y coordinates in the North, East, Down (NED) coordinate system (Bertaska et al., 2013) and the orientation ψ about z -axis (roll, pitch, and heave state variables are neglected in our application). The continuous space $X_{\eta} \times T$ was discretized to 4D state space S , where each discrete state is given by $\mathbf{s}_j = [x_j, y_j, \psi_j, t_j]^T$. Let the initial discrete state of the USV be given by $\mathbf{s}_I = [x_I, y_I, \psi_I, t_I]^T \in S$ and its final goal state given by $\mathbf{s}_G = [x_G, y_G, \psi_G, t_G]^T \in S$. The goal state can be constant or time varying depending upon the task performed by the USV.

Let $\mathbf{U}_c(\mathbf{x}_j) = \{\mathbf{u}_{c,1}, \mathbf{u}_{c,2}, \dots, \mathbf{u}_{c,M}\} \in \mathbb{R}^2 \times \mathbb{S}^1$ be the continuous, state dependent control action space, where each control action $\mathbf{u}_{c,k} = [u_d, \delta t, \psi_d]^T$ consists of the desired surge speed u_d , the execution time δt , and heading ψ_d in the NED system. These control actions are further used to map the state $\mathbf{x}_j \in X$ to its neighboring state $\mathbf{x}_{j,k} \in X$ for $j = 1, 2, \dots, |X|$, and $k = 1, 2, \dots, |\mathbf{U}_c(\mathbf{x}_j)|$. Let the discrete control action primitive set be represented by $\mathbf{U}_{c,d}(S) \in \mathbb{R}^2 \times \mathbb{S}^1$ in which each control action is given by $\mathbf{u}_{c,d,k} = [u_d, \delta t, \psi_d]^T \in \mathbf{U}_{c,d}(S)$.

Let the geometric region occupied by static obstacles be $\mathbf{O}_s = \cup_{k=1}^K o_{s,k} \subseteq \mathbb{R}^2$ and the geometric region occupied by OMT vessels be $\mathbf{O}_d = \cup_{l=1}^L o_{d,l} \subseteq \mathbb{R}^2$. Let the estimated state of the OMT vessels be given by $\{\mathbf{x}_{o,l} | \mathbf{x}_{o,l} \in X\}_{l=1}^L$. Let the 3 DOF dynamic model of the USV be $\dot{\mathbf{x}}_U = f_U(\mathbf{x}_U, \mathbf{u}_h)$.

Finally, a collision-free, dynamically feasible trajectory can be defined as $\phi : [0, t] \rightarrow X_{free}$ such that $\phi(0) = \mathbf{x}_I$ and $\phi(t) = \mathbf{x}_G$, where t is the execution time of the trajectory and $X_{free} = X \setminus X_{obs}$ represents the obstacle free region of the state space.

4.2.2. Global lattice-based trajectory planning

The global lattice-based trajectory planner as described in Švec et al. (2013) is an extension of our previous work presented in Švec et al. (2014c). The planner searches for a trajectory in a discrete 4D lattice structure L of the discretized state space S . At every expanded state \mathbf{s}_j , the control action primitive set $\mathbf{u}_{c,d} \in \mathbf{U}_{c,d}(\mathbf{s}_j)$ is used to determine its neighbors $\mathbf{s}_{j,k}$, where $j = 1, 2, \dots, |S|$ and $k = 1, 2, \dots, |\mathbf{u}_{c,d}|$. The lattice L consists of several 2D planning layers of x and y with constant orientation ψ and time t . Thus, each expanded neighbor $\mathbf{s}_{j,k}$ will transition to adjacent layers of the lattice with a different orientation ψ_j and corresponding increment in time t . The neighbors $\mathbf{s}_{j,k}$ is determined by approximating the end of each control primitive to be at the center of the corresponding cube of the lattice structure L (i.e., to ensure the continuity of the computed trajectory ϕ).

During the search, the states are expanded in the least-cost, heuristic, weighted A* fashion (Pivtoraiko et al., 2009) according to the cost function $f(\mathbf{s}) = g(\mathbf{s}) + \epsilon h(\mathbf{s})$, where $g(\mathbf{s})$ is the optimal cost-to-come from the USV's initial state \mathbf{s}_I to the currently expanded state \mathbf{s} and $h(\mathbf{s})$ is the approximated heuristic cost-to-go from the current state \mathbf{s} to the goal state \mathbf{s}_G , and ϵ is the inflation factor. The cost-to-come is calculated as $g(\mathbf{s}) = \sum_{l=1}^L l(\mathbf{u}_{c,d,l})$ over L planning steps, and $l(\mathbf{u}_{c,d,l})$ is the length of the control primitive $\mathbf{u}_{c,d,l}$. The cost-to-come is calculated as $g(\mathbf{s}) = \infty$, when any of the control primitive

$\mathbf{u}_{c,d,l}$ enters the obstacle region $S_{obs} \subset S$. The heuristic component $h(\mathbf{s})$ of the cost function helps to increase the speed of the search, and is approximated as the Euclidean distance between the current state \mathbf{s} and the USV's goal state \mathbf{s}_G . The inflation parameter $\epsilon \geq 1$, helps to find the right balance between the computational demand and the optimality of the computed trajectory. The final trajectory ϕ is composed of a series of dynamical feasible control action primitives $\mathbf{u}_{c,d,l}$, which are eventually converted into a series of waypoints $\{\mathbf{w}_i | \mathbf{w}_i = [x, y]^T\}_{l=1}^L$. The waypoints serve as local motion goals for the USV's low-level controller and the local VO-based planner (see Section 4.1.1).

4.2.3. Local velocity obstacle based COLREGs-compliant trajectory planning

The algorithm developed in this section is a local, COLREGs-compliant planner based on the Velocity Obstacles paradigm (Fiorini and Shiller, 1998; Kuwata et al., 2014). The local planning algorithms are primarily used to avoid the OMT vessels while optimizing the time to reach the local waypoint on the global trajectory ϕ computed by the global lattice-based planner. The standard VO-based approaches in Fiorini and Shiller (1998) and Kuwata et al. (2014) are unable to incorporate the dynamics of the USV into the planning. This leads to an increased collision rate in a dense, complex environment. The algorithms developed in this section integrate the dynamics and the low-level controller in the planning phase, which allows the USV to plan improved collision-free maneuvers. The mathematical details utilized by the algorithm are presented in Sections 4.2.3.1 and 4.2.3.2 below; first we provide an overview of the approach here.

As defined in Section 4.2.1, the phrase “control action primitives” is used to refer to a set of parameters that consists of a desired surge speed, execution time, and heading. The planner uses a dynamic model of the USV and its low-level controller to compute a large number of dynamically feasible control action primitives at each time step. To perform COLREGs-compliant avoidance maneuvers, the planner samples the dynamically feasible control primitives from the control action primitive set \mathbf{U}_c to identify a subset of collision-free and dynamically feasible, control action primitives $\mathbf{U}_{c,free}$. Collisions are determined by computing the distance and time corresponding to the closest point of approach (CPA) between the interceptor USV and any other moving traffic OMT vessels (see Fig. 5). The CPA distance (d_{CPA}) is the minimum distance that will occur between the USV and other vehicle if each of them maintains its heading and surge speed. The CPA time (t_{CPA}) is the time between the current time step and when the CPA occurs. If the computed CPA time is less than a user-defined minimum $t_{CPA} < t_{CPA,min}$ and the user-defined CPA distance is less than a user-defined maximum $d_{CPA} < d_{CPA,max}$, the control primitive is said to be colliding with the other vehicle. The parameters $t_{CPA,min}$ and $d_{CPA,max}$ are generally dependent upon the size, maximum surge speed, and maximum turning radius of the USV and are defined by the user.

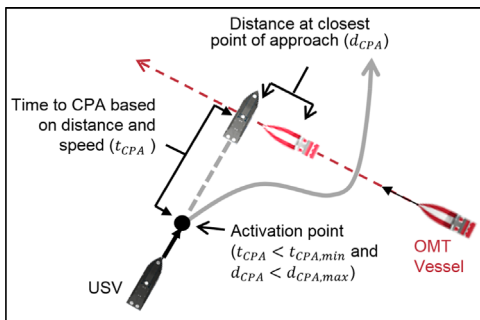


Fig. 5. Calculation of Closest Point of Approach (CPA) distance and time (i.e. d_{CPA} and t_{CPA}). The avoidance maneuver is activated when the CPA time and CPA distance are below user-defined thresholds (i.e. $d_{CPA} < d_{CPA,max}$ and $t_{CPA} < t_{CPA,min}$).

Once computed, $\mathbf{U}_{c,free}$ is used to identify COLREGs-compliant control actions (see Fig. 6). The appropriate COLREGs rule for each control action $\mathbf{u}_{c,d} \in \mathbf{U}_{c,free}$ is determined by the relative pose of the OMT vessel with respect to the interceptor USV. For example, the OMT vessel in Fig. 6 is in the cone of the green color and is said to be in a “crossing from starboard” situation.

Then, the cost of each collision-free control action primitive in $\mathbf{U}_{c,free}$ is calculated using the cost function described in Eq. (16) below, which takes into account the deviation from the global trajectory, the reduction in surge speed, and the COLREGs-compliance that would arise from the control action. The planner selects the control action with the lowest cost and converts it into a series of waypoints, which are then output to the low level controller.

4.2.3.1. Generalized Velocity Obstacles (GVO). The Generalized Velocity Obstacles technique described in Švec et al. (2013) incorporates the nonlinear dynamic model of the vehicle to determine obstacle regions in the control space. By performing simulations forward in time, the planner predicts the motion of the USV using its system-identified dynamic model $\dot{\mathbf{x}}_U = f_U(\mathbf{x}_U, \mathbf{u}_h)$ up to a specific user-defined time horizon t_{max} .

Firstly, the planner determines a set of control actions $\mathbf{U}_{c,free}(\mathbf{x}_U) = \mathbf{U}_c(\mathbf{x}_U) \setminus \mathbf{U}_{c,obst}(\mathbf{x}_U)$ that allow the USV to avoid collision zones. The set $\mathbf{U}_{c,obst}(\mathbf{x}_U) = \{\mathbf{u}_c | d_{CPA}(t_{max}) < d_{CPA,col}\}$, defines obstacles in the control space, where, as mentioned above, $d_{CPA}(t_{max})$ is the minimum distance between the closest point of approach (CPA) (i.e., the minimum distance of the USV from the OMT vessels) and obstacles when \mathbf{u}_c is executed from \mathbf{x}_U for the time horizon t_{max} . The distance $d_{CPA}(t_{max})$ is defined as $d_{CPA}(t_{max}) = \min_{t \in [0, t_{max}]} |\mathbf{U}(\eta_U(t)) - \mathbf{O}_d(t)|$, where $\mathbf{U}(\eta_U(t))$ is the geometric region in \mathbb{R}^2 occupied by the USV at $\eta_U(t)$, and $\mathbf{O}_d(t)$ is a region of time-projected obstacles. The motion and sensing uncertainty can be handled by adjusting the parameter $d_{CPA,col}$, i.e. the distance threshold of the USV from the OMT vessels. Secondly, the planner determines whether the USV, given its current pose, is in a COLREGs situation with respect to all other vessels, as depicted in Fig. 6. This is determined using the $d_{CPA}(t_{max}) < d_{CPA,min}$ and $t_{CPA}(t_{max}) < t_{CPA,max}$ conditions, where $d_{CPA,min}$ and $t_{CPA,max}$ are the user-specified distance and time thresholds. The time to CPA $t_{CPA}(t_{max})$ is defined as $t_{CPA}(t_{max}) = \arg\min_{t \in [0, t_{max}]} |\mathbf{U}(\eta_U(t)) - \mathbf{O}_d(t)|$. The variable $d_{CPA}(t_{max})$ is computed for the control action $\mathbf{u}_c = [u_d, 0]^T$ up to the maximum look-ahead time t_{max} , where u_d is the currently commanded surge speed to the USV.

If the above defined conditions holds and the USV is on the collision course with an OMT vessel, then we have to determine which one of the following COLREGs situations – i.e., “head-on,”

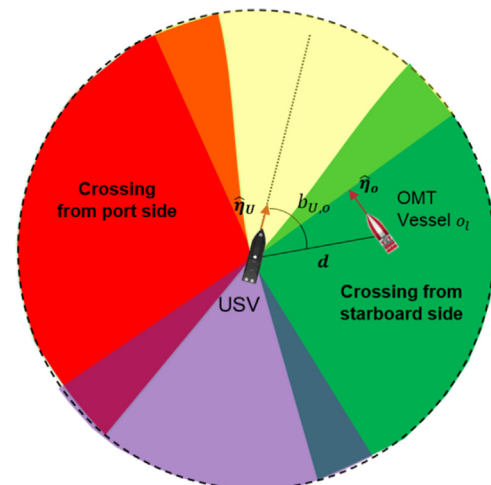


Fig. 6. COLREGs rule for each OMT vessel is determined by its current position with respect to the USV.

“crossing,” and “overtaking” (Commandant, 1999) – is valid with respect to all OMT vessels. An example showing one OMT vessel is presented in Fig. 6. This is useful for determining what constraints to apply on $\mathbf{U}_{c,\text{free}}$ to make the USV act according to the user's needs in a particular COLREGs situation. Let $b_{U,o} = 2\pi + \arctan((y_U - y_o)/(x_U - x_o)) - \arctan(n_{o,y}/n_{o,x})$ be the relative bearing of the USV to the OMT vessel, where $\hat{n} = [n_{o,x}, n_{o,y}]^T$ is the unit vector in the direction of the obstacle's heading ψ_o . Let $h_{U,o} = 2\pi + \arctan(n_{U,y}/n_{U,x}) - \arctan(n_{o,y}/n_{o,x})$ be the relative heading of the USV to the obstacle, where $\hat{n} = [n_{U,x}, n_{U,y}]^T$ is the unit vector in the direction of the USV's heading ψ_U . Both the values are required to be within $[0, \pi]$. The “head-on” situation is activated if $b_{U,o} \in [b_{h,\min}, b_{h,\max}]$, $h_{U,o} \in [h_{h,\min}, h_{h,\max}]$, the relative, along-track x coordinate of the obstacle in the body-fixed coordinate system of the USV satisfies $x_{o,U} \geq x_{h,\min}$, and the relative, cross-track y coordinate of the obstacle satisfies $|y_{o,U}| \leq y_{h,\max}$. The “overtaking” situation is activated if $h_{U,o} \in [h_{o,\min}, h_{o,\max}]$, $x_{o,U} \geq x_{o,\min}$, and $|y_{o,U}| \leq y_{o,\max}$. Finally, the “crossing from starboard” situation is activated if $b_{U,o} \in [b_{c,\min}, b_{c,\max}]$, $h_{U,o} \in [h_{c,\min}, h_{c,\max}]$ and $x_{o,U} \geq x_{c,\min}$.

If the USV is in a COLREGs situation with respect to any of the OMT vessel, the collision-free control action set $\mathbf{U}_{c,\text{free}}$ is divided into the COLREGs-compliant control action set $\mathbf{U}_{c,\text{COLREGs}}$ and the control action set that do not comply to COLREGs denoted by $\mathbf{U}_{c,\sim\text{COLREGs}}$. The subset $\mathbf{U}_{c,\text{COLREGs}}$ is determined based on the type of the current COLREGs situation and the future-projected possible states of OMT vessels relative to the current state of the USV. Let $\eta_U(t_0)$ and $\eta_U(t)$ be the poses of the USV at the current and the projected time respectively, and $\eta_o(t)$ be the pose of the obstacle at the projected time t . Let $\hat{n}_{U,o} = [n_{U,o,x}, n_{U,o,y}]^T$ be the unit vector in the direction between $\eta_U(t_0)$ and $\eta_o(t)$. Then, the control action u_c is considered to be COLREGs-compliant if $([n_{U,o,y}, -n_{U,o,x}]^T \cdot \hat{n}_{U,t_0,t}) < 0$, i.e., it leads the USV to the right half-plane between its current pose and the future projected pose of the obstacle.

Each control action in $\mathbf{U}_{c,\text{free}}(\mathbf{x}_U)$ is weighted using the cost function

$$\begin{aligned} \mathbf{u}_c^* = \operatorname{argmin}_{\mathbf{u}_c = [u_d, \psi_d] \in \mathbf{U}_{c,\text{free}}(\mathbf{x}_U)} \omega_u \left(\frac{u_{d,\max} - u_d}{u_{d,\max}} \right) \\ + (1 - \omega_u) \left(\frac{|\psi_w_j - \psi_d|}{2\pi} \right) + p_{\text{COLREGs}} \end{aligned} \quad (16)$$

where ω_u is the user-defined weight to balance between the surge speed error and heading error, $u_{d,\max}$ is the maximum surge speed of the USV, ψ_w_j is the heading towards waypoint \mathbf{w}_j on the planned global trajectory. Finally, $p_{\text{COLREGs}} = \omega_{CPA,t}/t_{CPA} + \omega_{CPA,d}/d_{CPA}$ is the additional penalty for the control action that is not COLREGs-compliant (Švec et al., 2013), where $\omega_{CPA,t}$ and $\omega_{CPA,d}$ are the user-defined weights. In other words, every control action from $\mathbf{U}_{c,\text{free}}$ is evaluated for its COLREGs compliance with respect to all the OMT vessels. The control actions that are COLREGs-compliant are always selected by the USV when available. However, the USV breaches the COLREGs rules to avoid collision when no COLREGs-compliant action is available.

4.2.3.2. Adaptive sampling-based GVO. The GVO-based planner samples the space of control action primitives to quickly determine a subset of control actions $\mathbf{U}_{c,\text{obst}}$ that may lead to a collision. This can be computationally expensive with the increase in the number of OMT vessels in the scene and the timing horizon t_{\max} . The adaptive sampling-based GVO algorithm described in Švec et al. (2014a) primarily depends on the pre-computed meta-model of the USV's dynamics and an associated low-level controller. This meta-model is represented as a 5D look-up table consisting of discrete, finite set of motion goals \mathbf{X}_G and corresponding trajectories Γ that leads to these goals from the current state \mathbf{x}_U of the USV. The algorithm uses this meta-model and searches for a motion goal that will avoid collisions

and minimizes the time to reach the local goal \mathbf{w}_j along the global trajectory ϕ . The resolution of the search space is iteratively increased during the search by expanding motion goals in the neighborhood of state space trajectories that lead to motion goals with the currently known minimum cost. Thus, the algorithm gradually discovers, with increasing resolution and focused sampling, an approximate representation of spatio-temporal obstacle regions in the state space. The motion goals are sampled non-uniformly along trajectories based on the difference in curvature between their consecutive segments, difference in surge speed, and the future projected poses of the OMT vessels. This reduces computation time, as a large number of states do not have to be evaluated for collision. As an example of the reduction in computational cost that can be achieved by extending this approach, simulations of the A* planner operating in waterways with multiple OMT vessels while maintaining COLREGs compliance have been performed and are available in Shah et al. (Submitted for publication).

4.3. Software architecture

The software architecture for these experiments required the tight integration of the low-level controller with the high-level planner. Several challenges needed to be addressed to create a reliable communication path between the two systems. The vehicle software architecture is Linux-based and written in C, while the planning software is Windows-based, and written in C++. Sufficient inter-process bandwidth is required for passing vehicle state information and receiving trajectories in real-time so that collisions with static obstacles or OMT vessels are avoided. The architecture must also be modular to permit the addition of future systems and subsystems.

4.3.1. Lightweight communications and data marshalling (LCM)

In designing the software architecture for the system, a reliable method of communication needed to be set up between the low-level controller and the high-level planner. This communication method requires cross-language and cross-platform support that allows the seamless, real-time communication from a Visual C++-based planner to a Linux-based vehicle control architecture. The LCM system was chosen as the basis for this architecture as current research into unmanned surface vehicles with an LCM-based operating system produced favorable results (Bingham et al., 2011). LCM is a communication protocol that relies on a publish/subscribe model to pass messages between processes and threads, known as inter-process communication (IPC). It utilizes a user datagram protocol (UDP) multicast to dispatch messages to all systems in scalable networks, thus negating the need for a main “server” mediator to arbitrate between subscriber and publisher. Furthermore, the choice of UDP allows for a fast data transfer rate with failed messages simply being dropped, without being checked by the publisher, as in transmission control protocol. The fast update rate commonly found in robotic systems allows for this error, as the failed message rarely causes a non-negligible system response (Bertaska et al., 2013).

4.3.2. System architecture

Fig. 7 displays the vehicle software architecture with the implementation of LCM. Each sensor described below in Section 4.4 is handled by a separate driver operating in parallel and has an exclusive LCM channel. These drivers parse the sensor information from the serial ports, condense the data into an LCM package, and distribute it to the appropriate LCM channel. All sensor information is handled by the USV's state estimator, which collects and organizes filtered state data into a separate package, which is then transmitted directly to the high-level planner via a separate LCM

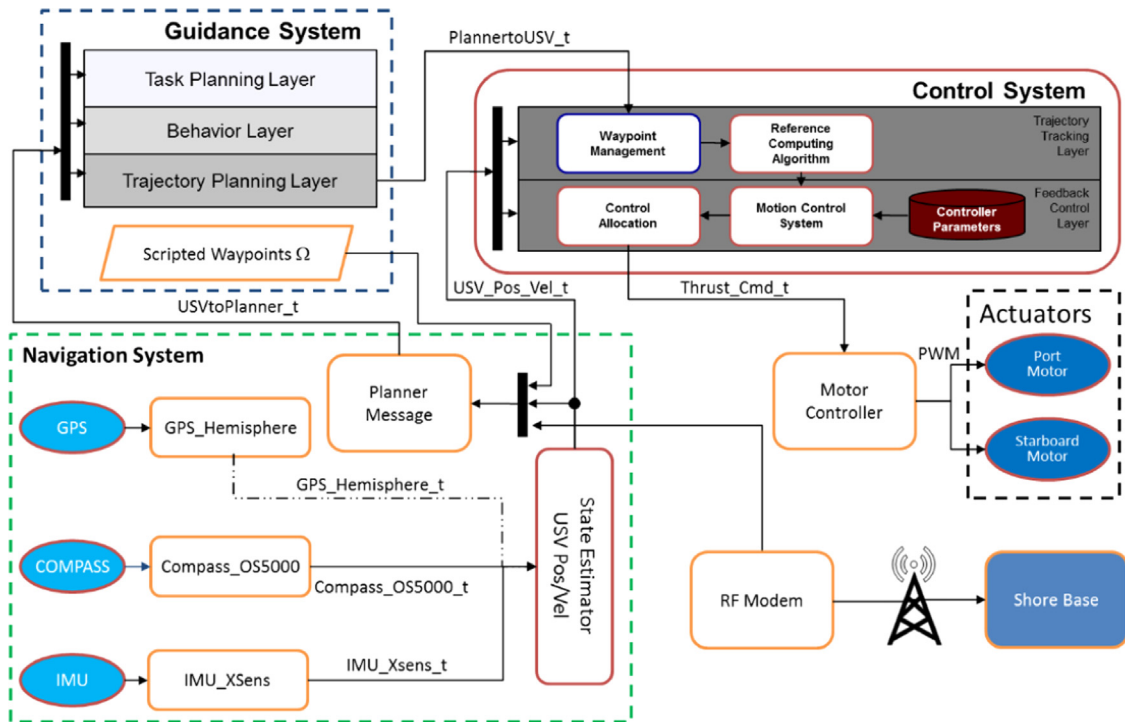


Fig. 7. Software architecture interfacing the high-level planner and low-level controller. All communication was handled through the Lightweight Communications and Data Marshalling (LCM) libraries, as it provided cross-platform and cross-language support with low latency and high bandwidth.

channel. Along with vehicle telemetry, this vehicle state LCM package includes an overall goal for the high-level planner. This goal may be either static or dynamic, depending on whether an “Approach” or “Following” behavior is being utilized. The end goal consists of a desired position in the NED coordinate system, as well as a desired endpoint heading.

Once the estimated state and goal are established and transmitted, the high-level planner produces a dynamically feasible trajectory from a referenced dynamic model of the vehicle. For these experiments, it was assumed that USV had perfect knowledge of the locations of the dynamic and static obstacles. The latter was known *a priori*. The LCM package containing the trajectory was set up as a variable length array, transmitting the desired locations in the NED system and desired surge speed to achieve those waypoints. Several parameters could be set “on-the-fly” to govern the distances between consecutive waypoints and how far off current course they may be. Trajectories received by the low-level system were broken down into discrete sets of waypoints and a LOS maneuvering system was employed to guide the vehicle to within a user-set minimum acceptable distance of each waypoint (Bertaska et al., 2013).

4.4. Control electronics and sensors

A combination of two hardware systems were implemented on the autonomous vehicles, where the low-level architecture was contained within an automatic control box, and the high-level planner was run on an onboard laptop computer.

In order to conduct development and testing of autonomous control for the USVs, a guidance, navigation, and control (GNC) hardware system was developed, consisting of a central control computer and sensor suite housed within an IP-67 rated plastic box (Fig. 8). The central computer was chosen to be the Technologic Systems TS7800, an ARM9-based, 500 MHz single board computer (SBC) running the Debian Linux distribution. The sensor suite comprised an inertial measurement unit (IMU) with global

positioning system (GPS) capability, tilt-compensated digital compass, RF transceiver, and pulse width modulation (PWM) signal generator. Vehicle state information was obtained from the compass and GPS-enabled IMU, which processed raw data through an enhanced Kalman filter before relaying it to the SBC. Likewise, the digital compass was internally low-pass filtered. A key feature of this command and control console is its modularity, where it may be interfaced with all four vehicles with little to no configuration. A detailed summary of the GNC sensor suite can be found in Bertaska et al. (2013).

Vehicle telemetry was transmitted through a radio frequency (RF) modem, where it was relayed to a base station. There, vehicle state information was logged and displayed in real-time on a graphical user interface (GUI). A router was also present within the automatic control box to allow wireless connection to the network, as well as remote access from shore at close distances (< 100 m). A 12-channel servo controller was used to switch control authority of the vehicle between a hand-held RC transmitter and onboard computer control. Thus, it was possible for a user to override the onboard computer control of the vehicle and manually steer it in case of an emergency.

The high-level planner was implemented on a Lenovo ThinkPad T420 running Windows 7. This laptop ran on an Intel i5 processor with 2.5 GHz and 8GB of RAM and was installed onboard the vehicle. This computer was wirelessly networked with the TS7800.

5. Experimental apparatus and procedures

5.1. Manned and unmanned surface vehicles

A combination of manned and unmanned systems was used in the field trials. However, each experiment was restricted to one autonomous system to accurately characterize the behavior of the

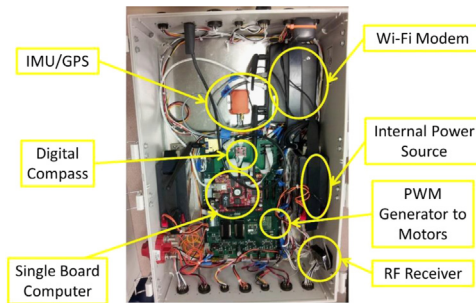


Fig. 8. Navigation and control hardware contained within the automatic control box.

high-level planner and low-level controller. The unmanned vehicles were either autonomously piloted or remotely controlled from shore.

Two systems were outfitted with the high-level planner/low-level controller software suite. Naturally, the control and planning parameters for each of these systems varied with the different maneuvering characteristics of each vehicle. The transition from one vehicle to the other mirrored the growth in intricacy in the goals of the experiments, as a higher top-speed with tighter turning characteristics was needed to employ “Following” and COLREGs-compliant behaviors. The “Approach” task stressed the compatibility of the high-level planner and low-level controller, and through the nature of the problem, did not contain a speed requirement. In such a case, a vehicle with a low top speed, such as the DUKW-Ling, may be used to adequately capture the mission. For the “Following” and COLREGs-compliant behaviors, speed was imperative in tracking the target and maintaining consistency with COLREGs rules. These experiments called for the use of a more maneuverable system with a higher top speed, the USV14.

The two manned and remote control systems were used as OMT vessels and adversarial targets in field trials. Under the adversarial role, one system navigated around the static obstacle course in the mission area as a target USV, while an autonomous system performed the “Following” operation as an interceptor USV. The manned OMT vessel was used to initiate a sequence of COLREGs situations to test the performance of the planner on the interceptor USV for COLREGs-compliant crossings.

5.2. DUKW-Ling

The 8.8 foot (2.7 m) DUKW-Ling (Fig. 9) is a 1/7th scale model of a tracked amphibious vehicle design concept called the DUKW-21 (Marquardt et al., 2014). The vehicle features a small waterplane area twin hull (SWATH) design, where most of the buoyancy of the system is submerged, allowing for a smaller waterplane area. This cuts down on the heave motion produced by wave effects. Experiments in this paper exclusively utilized its waterborne configuration, where a pair of two-bladed 12 V electric trolling motors propelled it in water. Each propulsion unit was capable of delivering up to 133 N of thrust. No rudder was present on the vehicle – thus, differential thrust was used to create a torque to turn the vehicle. Table 2 displays important properties of the DUKW-Ling used in tuning planning and control parameters.

5.3. USV14

The 14 foot (4.3 m) Wave Adaptive Modular Vessel (WAM-V), or USV14 (Fig. 10), is a twin hull pontoon style vessel designed and built by Marine Advanced Research, Inc. of Berkeley, CA. The vessel structure consists of two inflatable pontoons, two motor pods, a payload tray, and two supporting arches. Each pontoon has an independent suspension system whereby one is allowed to pivot freely of the other. This safeguards the payload tray from the

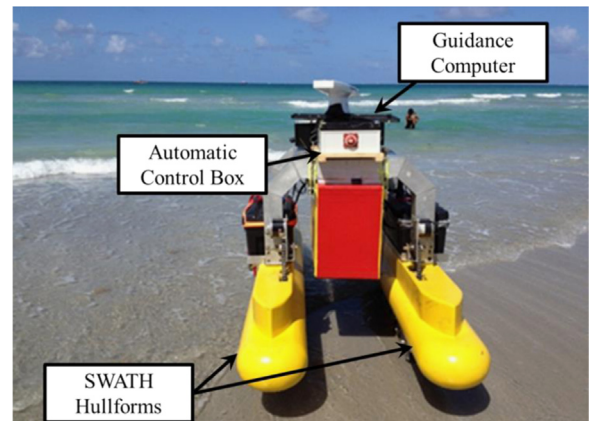


Fig. 9. DUKW-Ling on shore.

Table 2
DUKW-Ling properties.

| | |
|---------------------------------|---------|
| Maximum top speed | 1.0 m/s |
| Maximum thrust from motors | 266 N |
| Minimum turning circle diameter | 10 m |

effects of wave disturbances, when compared to a traditional catamaran design with stiff connections at each demihull (Klinger et al., Submitted for publication).

It is propelled by two 22.2 V waterjet engines, fixed and pointed directly aft. Due to this configuration, the vehicle is underactuated. Like the DUKW-Ling, the USV14 also relies on differential thrust to maneuver. However, the ability to produce negative thrust was not taken into account during control allocation, as the reversing buckets were neglected in the formulation of the control law. Table 3 displays important vehicle characteristics taken into consideration in deriving the planning algorithm and control law.

5.4. USV12

The 12 foot (3.7 m) WAM-V, or USV12 (Fig. 11), is a smaller version of the USV14 with many of the same design features. Similarly, it is a twin-hulled platform with independently pitching pontoons to mitigate wave disturbances on the superstructure. The vessel is propelled by two waterjets (each waterjet is driven by a 36 V electric motor) that deliver a total of 200 N. The USV12 has a top speed of 3.6 m/s. Although capable of running autonomous operations, this vehicle was restricted to remote control such that the planner could be tested in situations that elicited a greater variety of behaviors.

5.5. Johnboat

The 14 foot (4.3 m) johnboat is a manned vessel used in these experiments as a safety boat as well as an OMT vessel. Although not pictured in Fig. 12, it was furnished with the same sensor suite as shown in Fig. 8 to accurately give its position, heading, and speed.

6. Results and discussions

Field trials of the low-level controller and high-level planner were performed in a 750 m × 150 m enclosed area in a section of the US Intracoastal Waterway in Hollywood, Florida USA. Selection of the mission area was vital, as it had to possess favorable characteristics: a low level of boat traffic, protection from currents,

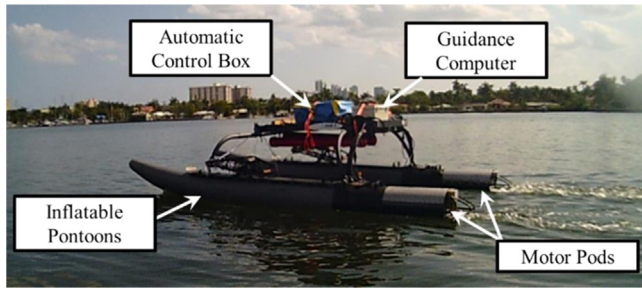


Fig. 10. The USV14 on the US Intracoastal Waterway.

Table 3
USV14 properties.

| | |
|---------------------------------|---------|
| Maximum top speed | 2.8 m/s |
| Maximum thrust from motor pods | 205 N |
| Minimum turning circle diameter | 12 m |

and moderate protection from wind and wave disturbances. Part of the aim of these experiments was to characterize the behavior of the vehicles in a non-ideal environment, where environmental forces were present, but not debilitating. To test the capabilities of the planner, the GPS coordinates of a set of static obstacles was generated in the mission area. Around each static obstacle a boundary zone (BZ) was also generated, the borders of which were marked by buoys during the field trials for visual feedback. The BZs formed buffer regions around the static obstacles. When a BZ was breached, the planner's priority was to navigate the vehicle out of the BZ. If the vehicle had encroached upon any static obstacles during a mission, the mission would have been terminated and the planner would have generated no new trajectories. This is analogous to a yellow/red traffic light situation while driving. The BZs acted like yellow traffic lights and were avoided, but no harsh penalties were incurred if a BZ was breached. On the other hand, static obstacles functioned as a red light for the mission, which would be terminated whenever a static obstacle was encroached upon. It should be noted that the vehicles encountered no static obstacles during the experiments. The configuration of the static obstacle fields became more complex as the goals of each experiment increased in difficulty. The results of simulation experiments performed using the developed lattice-based planner are presented in our previous work ([Švec et al., 2014c](#)) and in our recent work ([Shah et al., Submitted for publication](#)).

6.1. Experiment 1—“Approach”

The first experiment performed was that of an “Approach” behavior, where a USV would advance towards a reference point in a static obstacle-laden field. The “Approach” behavior constitutes a maneuver typical of a scenario where a USV would advance towards a target vessel in a static position. This example can be illustrated by a security USV approaching a moored suspect vessel. For the field trials conducted here, the pose of the suspect vessel was mocked by a reference GPS point. Several of these approach points were placed within the static obstacle field, and the USV was tasked with following them in a consecutive order. The vehicle used in these experiments was the DUKW-Ling.

As outlined in [Section 4.1.1](#), a simple heading proportional controller was utilized for the “Approach” behavior tests in Experiment 1. The planning algorithm used for this behavior is the global lattice-based planner (see [Section 4.2.2](#)). The global planner searched for a collision-free trajectory in 3D instead of 4D. We did not consider the time dimension for this set of

experiments because the environment only contained static obstacle regions. The positions of all the static obstacles were provided as *a priori* knowledge to the planner. The planning space was discretized into a 2D grid with a resolution of 1 m. The orientation of the USV was discretized into 8 levels, each of 0.785 rad.

The control action primitive set contained three control actions $\mathbf{u}_{c,d} = [u_d = 1.5 \text{ m/s}; \delta t = 5 \text{ s}; \psi_d = -0.785, 0, +0.785 \text{ rad}]$. The control primitives are designed such that the approximate length of each action primitive is about 7 m, which can be successfully executed by the DUKW-Ling platform. The radius of the region-of-acceptance around all the waypoints as well as the checkpoints was set to 15 m. If the vehicle fails to reach a specific waypoint by small margin due to change in environment disturbances, then it has to perform one complete loop to reach back to the same waypoint. The high acceptance region always allowed the USV to reach waypoints under wide range of environmental disturbances and avoids undesired looping during the execution of the planned path. The inflation factor ϵ was set to 1.5 to ensure good quality trajectories with low computation time ([Bertaska et al., 2013](#)).

6.1.1. Experiment 1—“Approach” results

Three tests were run with this configuration over a course of days with varying environmental conditions. The control law for the DUKW-Ling was set to different forward motor biases, ranging from 40% to 70% of full-scale throttle. A sample mission is presented in [Fig. 13](#), representative of all trials for the “Approach” behavior (discrepancies were caused by changes in environmental conditions and motor bias). Approach points are marked by red circles, static obstacles by blue circles, trajectory waypoints by green circles, and the path taken from the USV by the black line ([Fig. 13a](#)). The USV ran the course according to the trajectory it received from the planner. This trajectory was recomputed every 20 s or when the vehicle was a set distance away from an approach point ([Fig. 13b](#)). At the end of each leg, a new goal was generated, and the vehicle progressed to the next objective ([Fig. 13c](#)). The planner successfully navigated the USV around the static obstacle field with minimal BZ encroachment and followed the sampled path depicted in green in [Fig. 13](#). The location of the second approach point in the northwest quadrant stressed planner capabilities, as it had to successfully turn the vehicle 180° in a tight waterway. Therefore, the model referenced by the planner had to follow vehicle dynamics ([Fig. 13d](#)). This was successfully completed, and the DUKW-Ling navigated to the last approach point before returning to the shore base ([Fig. 13f](#)). In general, the test was successful as communication between the planner and vehicle control architecture was uninterrupted and the planner guided the USV around the course during every mission. Results are shown over the course of three runs in differing environmental conditions in [Table 4](#). The majority of the BZs were avoided for the three approach points, with encroachment occurring only around the outer edges of the eastern-most BZ. This can be attributed to the environmental conditions in that area, where the vehicle was the closest to a north-south channel under a current. As described in [Section 4.1.1](#), the more motor capacity that was devoted towards propelling the DUKW-Ling, the less steering torque it had available to maneuver. This caused the tests with a lower motor biases to avoid more BZs than those with higher motor biases.

Overall, the vehicle avoided the overwhelming majority of the BZs and all static obstacles, as well as transiting to within a user-specified distance of each approach point. Respective goals from the control level layer and the planner were achieved, thus allowing for the expansion of the current system to include the “Following” behavior, as is shown in the proceeding section.

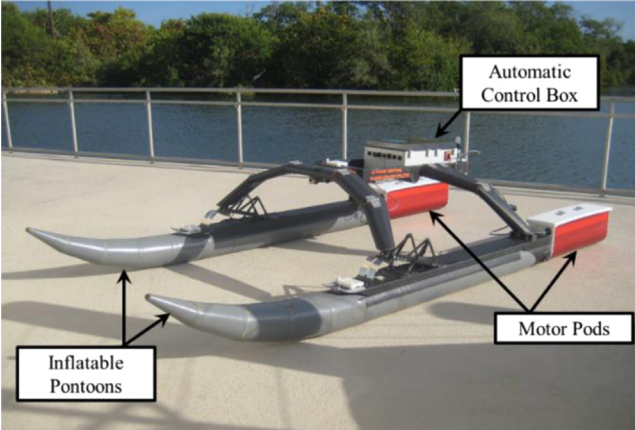


Fig. 11. The USV12 onshore.



Fig. 12. The manned johnboat.

6.2. Experiment 2—“Following”

The next experiment tested the “Following” capabilities of the planner, where an interceptor USV chased a target vessel in the same static obstacle field. This differed from the approach field trial, as the end goal of the USV was now a dynamic point. Three vehicles were utilized in the two different roles for this experiment. The autonomous USV now had a speed requirement to successfully get within a 30 m ring of the moving target. Due to this constraint, the USV14 was chosen as the autonomous platform, and the USV12 and johnboat were alternated as the target vessel. Both were under manned control, either through remote control (USV12) or an on-board captain (johnboat).

The same static obstacle field used the “Approach” experiment was also used for the “Follow” tests, and the target vessel ran a similar course (Fig. 14). For the USV14 to maintain a set distance from the target, an outer/inner ring for a desired motion goal was set around the target, where once the chase USV entered the ring, its surge velocity would slowly degrade to nearly zero. If it entered the inner circle around the target vehicle, a collision was imminent, and emergency stop procedures were enacted. The target vessel varied its speed at different points in the course to simulate aggressive maneuvering, and test the responsiveness of the USV14.

The chase USV was assumed to have perfect knowledge of the location and orientation of the target. To simulate this system, the vehicles communicated telemetry over RF transceivers. These were relayed in an ASCII-based, NMEA0183 string with vehicle identifiers. This was received by the chase USV's low-level software architecture and packaged into its state LCM message as the goal of the trajectory. The RF transmissions were displayed on the GUI and logged at the base station.

As discussed in Section 4.1.2, a combined proportional heading and proportional surge speed controller was used to control the

vehicle during the “Following” behavior experiments. The planning algorithm used for these tests is the global lattice-based planner described in Section 4.2.2. This planning algorithm searches for a global trajectory in 4D including the time dimension. Unlike the trajectory planning algorithm used for the “Approach” behavior, this algorithm has a time varying goal location (i.e., the moving target boat). Thus, the planner has to vary the surge speed of the USV14 while planning the global trajectory in order to successfully follow the target boat. The final motion goal \mathbf{x}_G for the planner was placed 30 m behind the target boat to ensure safety. The control action primitive set $\mathbf{u}_{c,d} = [u_d, \delta t, \psi_d]$ consisted of 9 primitives (3 levels of surge speed and 3 levels of heading) and was designed to have constant travel distance of 7 m. Hence, the primitives with high surge speed (u_d) have low values of execution time (δt) and vice versa. The USV14 was operated at the maximum surge speed of 1.7 m/s for this set of experiments.

6.2.1. Experiment 2—“Following” results

The experimental results of the follow task is shown in Fig. 15. During the experiment, the USV14 employed the deliberative trajectory planner to compute a dynamically feasible trajectory to a motion goal positioned 30 m directly behind the target boat. The goal pose was updated as the USV14 received new transmissions from the target vessel. If the interceptor was outside of the 30 m ring, it would actively chase the target. If it was within 30 m, it would slow down and maintain that set distance (Fig. 15h-j). As shown in Fig. 15a, the USV14 avoids a static obstacle when approaching the target from its initial location. Fig. 15b illustrates a situation in which the target boat increases its speed to 1.5 m/s, causing the USV14 to accelerate to a matching speed in order to maintain the required distance. In Fig. 15e-f, the target boat quickly reduces its speed to 0.5 m/s, which forces the USV14 to respond appropriately by cutting throttle and coasting to a near complete stop. Motion goals set by the planner were achieved in that the proportional control law followed the reference speed (Fig. 15i), and successfully decelerated when the distance to the target vessel dropped below 30 m (Fig. 15h-j). Table 5 displays the results of three runs of the “Following” experiment over different planner-limited top speeds and environmental conditions. It is easy to see that the USV14 was less susceptible to changes in environmental conditions when compared to the DUKW-Ling, as all three runs displayed similar results.

6.3. Experiment 3—COLREGs-compliant crossings

Three different scenarios were tested for compliance with COLREGs. These were selected in their applicability to realistic situations, where a USV may need to navigate around several moving and moored obstacles. The size of the mission area was reduced from previous tests in order to constrain the vehicles so that they were operating in a tight waterway. Static obstacles were present in the northern, southern, and western boundaries. During all three tests, the vehicle was programmed to approach a point at the northwest quadrant of the mission area. As the interceptor USV traversed the static obstacle field, a human-operated vessel (johnboat) would interfere in its path in a COLREGs-appropriate manner.

Three different interference patterns were simulated and tested on the water. The first was a “head-on” crossing scenario, where the OMT vessel approaches the USV head-on. According to COLREGs, this would require a port-to-port crossing where the USV would gently deviate to the right from the trajectory of the human-operated vessel, and then follow its course to the destination (Fig. 16a). Second was a “crossing from starboard” scenario, where at approximately the halfway point of the USV's path, the OMT vessel crosses the USV path from the USV's starboard side almost at right angle to the latter. This constitutes a crossing situation, and

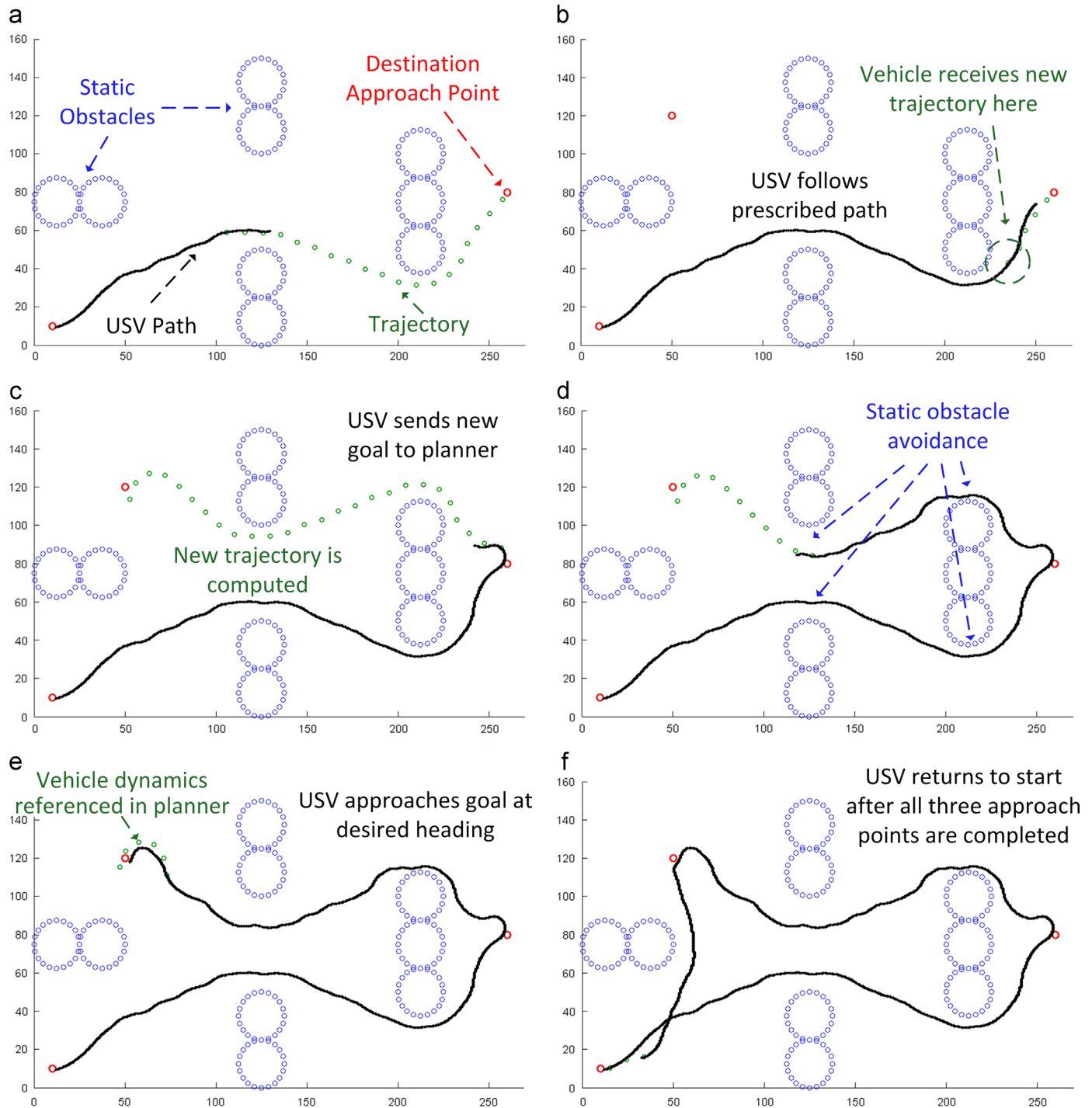


Fig. 13. "Approach" experiment results with the DUKW-Ling at 40% motor capacity. (For interpretation of the references to color in this figure legend, the reader is referred to the web version of this article.)

Table 4

Results of the "Approach" behavior over three runs with varying motor biases and environmental conditions.

| Run number | Motor % for surge speed (%) | Number of BZ incursions | Average sustained wind speed (m/s) | Average Wind Gust (m/s) |
|------------|-----------------------------|-------------------------|------------------------------------|-------------------------|
| 1 | 40 | 2/9 | 4.5 | 6.0 |
| 2 | 60 | 2/9 | 5.3 | 7.1 |
| 3 | 70 | 3/9 | 5.8s | 8.1 |

the USV is required to yield to the approaching OMT vessel (Fig. 16b). Lastly, an "overtaking" scenario was tested, where the faster-moving USV passes a slower-moving OMT vessel. It is typically required that a faster moving vehicle overtakes a slower vehicle on the latter's port side; however, under certain circumstances, overtaking on the starboard side of the slower vehicle is allowed. The configuration of the static obstacles in the field made it simpler to do so on the starboard side of the OMT vessel (Fig. 16c).

Due to the speed and maneuvering requirements for performing these movements, the USV14 was chosen as the autonomous

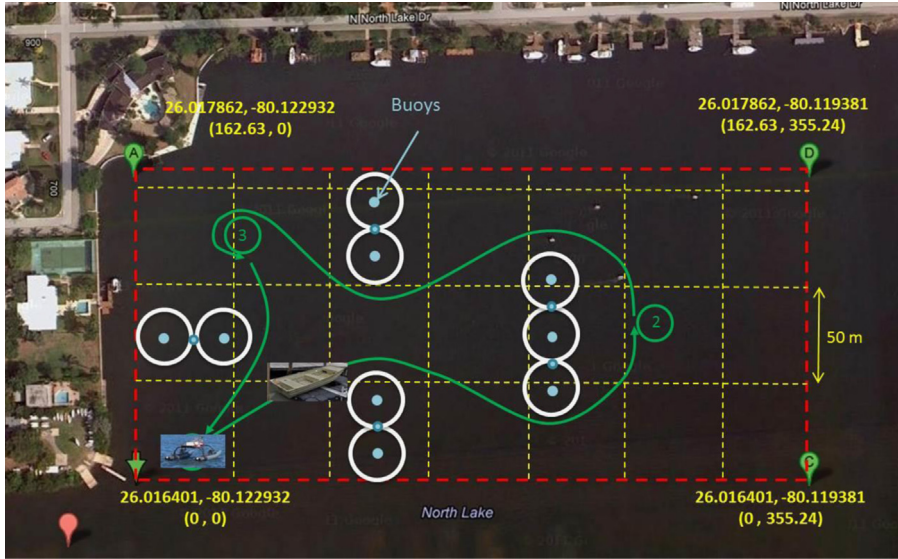


Fig. 14. Course configuration for the “Approach” and “Following” experiments (Bertaska et al., 2013).

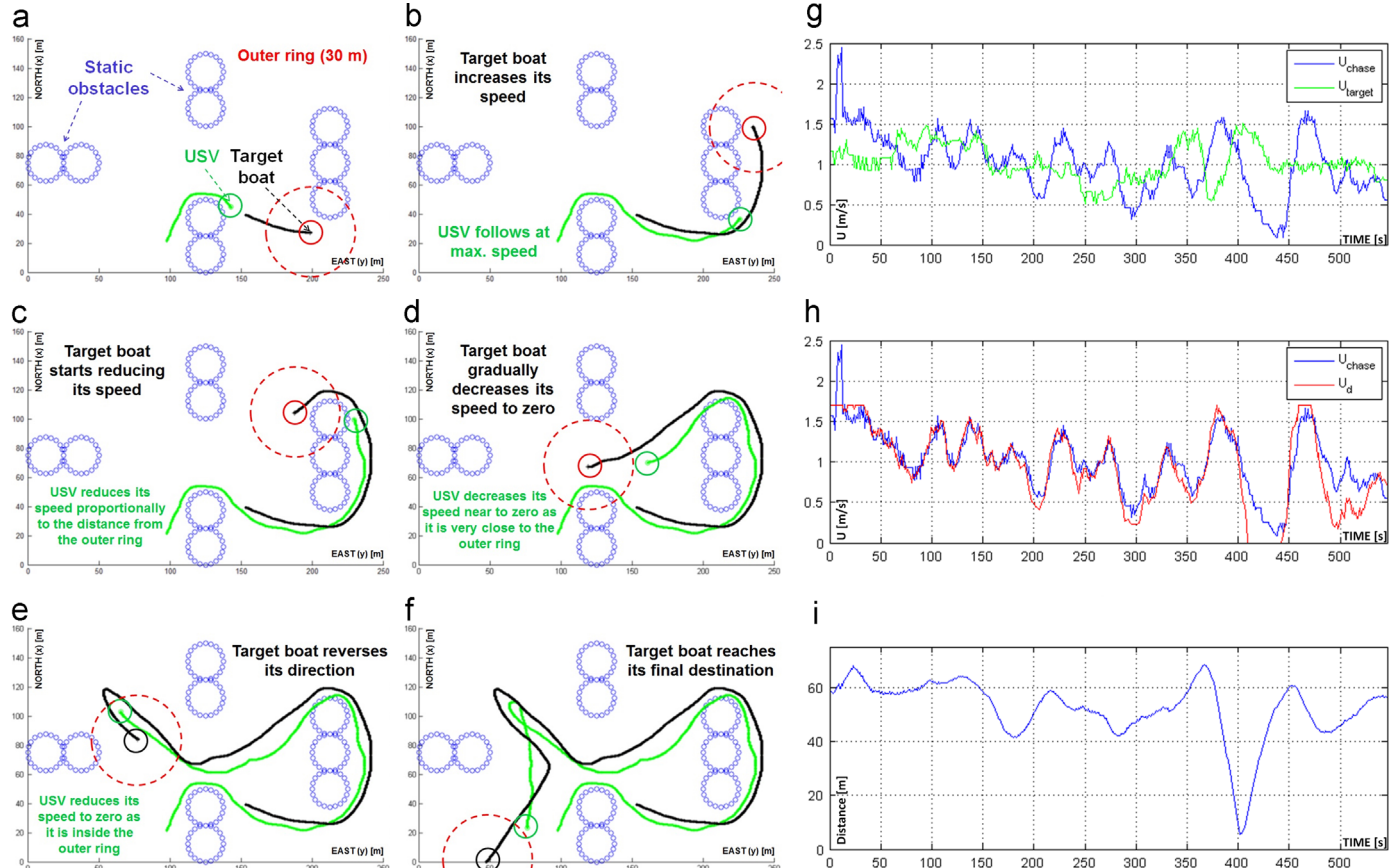


Fig. 15. Results of the “Following” experiment at different points of the map. As in the previous figure, the blue points are virtual obstacles and the green line is that of the USV. The black line is of the target vessel’s path, which the USV is matching throughout the course. Vehicle behavior in response to the planner is shown in (h) and (i). Distance between vehicles is displayed on (j). (For interpretation of the references to color in this figure legend, the reader is referred to the web version of this article.)

platform equipped with the high-level planner. The static obstacle field was reduced to maximize the maneuverable area of the test site, while still maintaining a constraint of a narrow waterway. For every scenario, the USV would start near the southern edge of the map and then navigate to a point in the northwest quadrant.

Due to the speed and heading requirements of performing these maneuvers, the same proportional control law as in the “Following” experiment was used. The computational demand of

the Generalized Velocity Obstacle (GVO) based planner described in Section 4.2.3.1 was significantly higher compared to the other planners. Due to the lack of high performance computing hardware, we used the classical VO-based planner (Fiorini and Shiller, 1998; Kuwata et al., 2014) with a modified cost function to enforce COLREGs rules while performing the experiment. The CPA parameters ($t_{\text{CPA}, \max} = 50$ s and $d_{\text{CPA}, \min} = 60$ m) were used to determine all the OMT vessels that are on the collision course with the

USV14. The algorithm checks for the appropriate COLREGs rules applicable with respect to each OMT vessel and penalizes all of the collision velocity vectors accordingly (Švec et al., 2013).

6.3.1. Experiment 3—Results

The experimental results of the COLREGs-compliant obstacle avoidance is shown in Fig. 17. In these experiments, the USV14 employed the reactive, local planner to determine a dynamically feasible, COLREGs-compliant control action to approach a local waypoint of the trajectory. During a run, the speed of the OMT vessel was kept constant, although the constant speed selected for each scenario was different. Fig. 17a and b depict the result of COLREGs-compliant obstacle avoidance in the “head-on” situation. In this experiment, the USV14 headed towards a virtual target vessel positioned in the top left corner of the scene at a nominal speed of 1.5 m/s. The OMT boat headed southeast at 0.8 m/s. The boats were intentionally positioned to be on a collision course. The USV14 successfully yielded to the OMT boat by slowing its motion to 1.3 m/s and steering to starboard to avoid the OMT vessel on its port side.

Fig. 17c and d depict the result of COLREGs-compliant obstacle avoidance in the “crossing from starboard” situation. In this experiment, the OMT vessel headed eastward at 0.5 m/s. Its speed and initial pose was set such that it was on a collision course with the USV14. The USV14 successfully yielded to the OMT vessel by slowing down from 1.5 m/s to 0.7 m/s, allowing for the OMT vessel to pass, and avoiding it on its port side. Finally, Fig. 17e and f depict the result of COLREGs-compliant avoidance in an “overtaking” situation. In this experiment, both of the boats headed northward, with the OMT maintaining course and speed, which was decreased to 0.5 m/s. The USV14 successfully carried out the required maneuver of passing the OMT on the starboard side, due to the constraints of the obstacle field, and then continuing to its final motion goal. After execution of each avoidance maneuver, the USV14 switched back to the global, deliberative trajectory planner and proceeded towards the virtual target vessel. Table 6 displays the results from this experiment when compared to environmental conditions during those tests. It should be noted that although no BZs were entered, they did limit the ability of the planner to generate trajectories to avoid the OMT.

Table 5

Results from “Following” experiment compared against environmental data during runs.

| Run number | Max top speed (m/s) | Number of BZ incursions | Average sustained wind speed (m/s) | Average wind gust (m/s) |
|------------|---------------------|-------------------------|------------------------------------|-------------------------|
| 1 | 1.5 | 3/9 | 2.1 | 4.4 |
| 2 | 1.5 | 2/9 | 4.5s | 6.8 |
| 3 | 1.7 | 3/9 | 5.4 | 7.0 |

6.4. Experiment 4—approach behavior with multiple COLREGs crossings

Operating a USV in a crowded waterway while following the COLREGs presents multiple challenges. Successful avoidance of one OMT vessel may cause a chain reaction of collisions that occur later with other OMT vessels or static obstacles. Some situations may call for a breach of the COLREGs to prevent near certain collisions that would occur if the COLREGs were strictly followed. The ensuing test featured multiple COLREGs crossings at varying incoming angles relative to the USV and an updated planning algorithm and control system to improve vehicle and planning performance.

A new static obstacle field was created that more closely resembled a traditional waterway (Fig. 18). A series of approach points were selected as in Section 6.1 for the USV to follow (Fig. 18a). The USV would navigate through the obstacle field according to those approach points, followed by two sequential COLREGs crossings. During these transitions, a manned OMT vessel (johnboat) initiated the local reactive planner to perform a COLREGs-compliant crossing (e.g. Fig. 18b). The OMT vessel then removed itself from the area of the reactive planner and returned at a different angle causing another COLREGs-compliant crossing (e.g. Fig. 18c). Two of these crossings were performed for each of five runs in the transition between the third and final approach points (Fig. 18d). A single human-operated vehicle, in lieu of multiple vehicles, was used to simplify the coordination and implementation of the physical experiments. The simulation experiments presented in Švec et al. (2013) and (2014a), demonstrates that the developed algorithms are capable of handling COLREGs scenarios with multiple vehicles. A top speed of 2 m/s was set for the USV14, which was its nominal speed for the global deliberative planner, while the local reactive vehicle speed varied according to given COLREGs situations. As discussed in Section 4.1.3, a nonlinear backstepping controller was used for the multiple COLREGs-compliant crossing tests. This experiment utilized planning algorithms that are a combination of the lattice-based global planner described in Section 4.2.2 and the adaptive sampling-based GVO local planner described in Section 4.2.3.2. The global planner is used to compute trajectories with minimum travel time and distance to reach the global goal and also avoid static obstacles in the scenario. The local planner has very high replanning rate and is used to perform COLREGs-compliant OMT avoidance. The planning algorithm switches from the global to local planner when CPA parameters (t_{CPA} , d_{CPA}) with respect to any of the OMT vessels fall below the user-specified threshold, i.e. $t_{CPA} < t_{CPA, max}$ and $d_{CPA} < d_{CPA, min}$. The values of these parameters were tuned during the experimental runs and were set to $t_{CPA, max} = 50$ s and $d_{CPA, min} = 60$ m. Both the local and the global planner had prior knowledge of the static obstacle regions. The control action primitive set for the global planner is same as that of the “Follow” behavior described in Section 6.2.1 (Švec et al., 2014a).

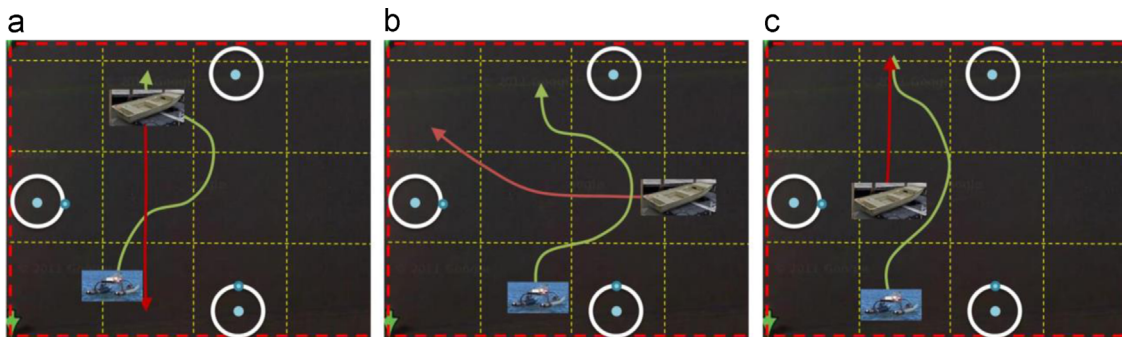


Fig. 16. Experiment 3 objectives and course configuration: “head-on” crossing (a), “crossing from starboard” (b), and “overtaking” (c) COLREGs scenarios. The USV14 will perform the COLREGs-compliant crossings in the obstacle field shown above.

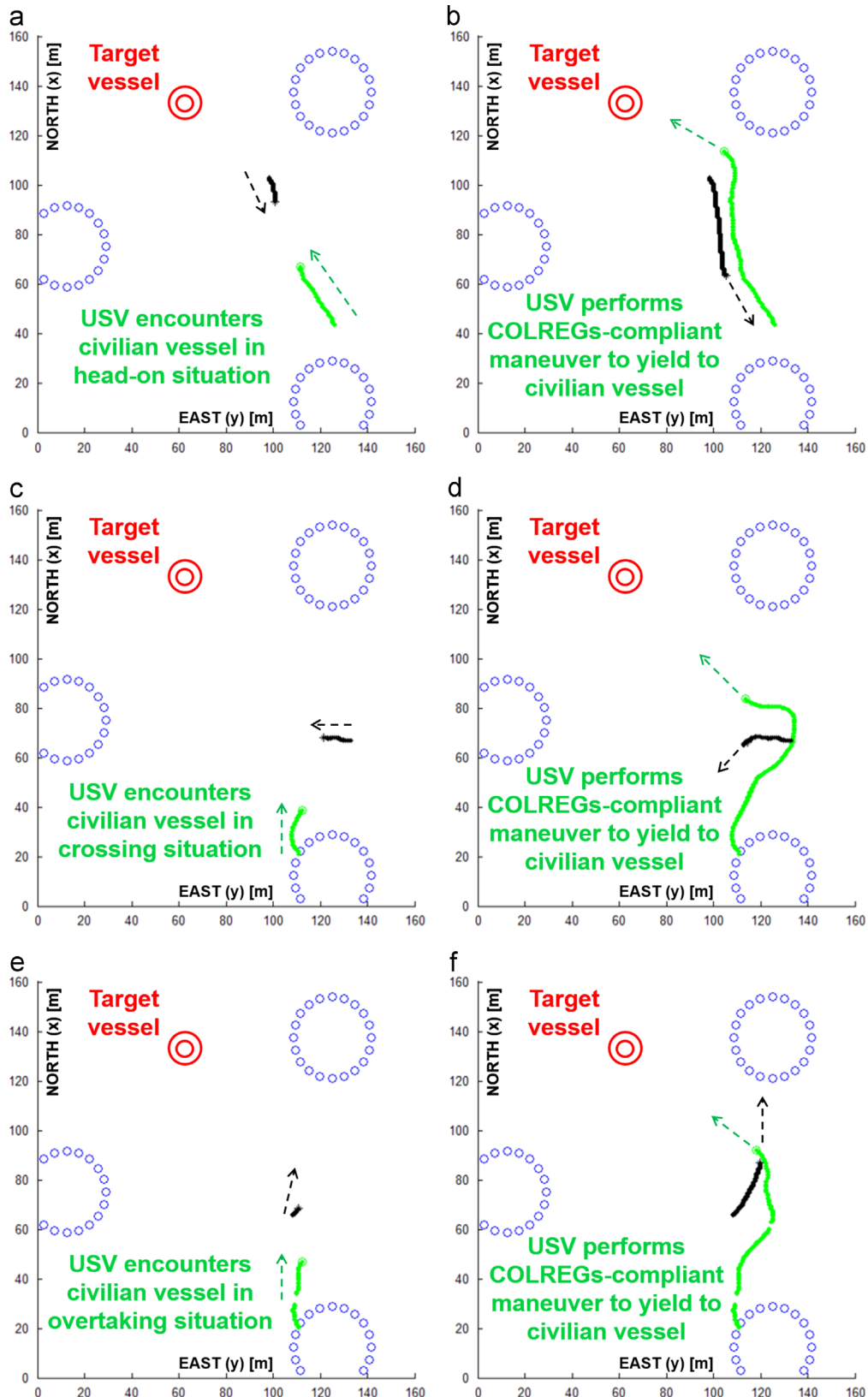


Fig. 17. Experimental results of the COLREGs-compliant obstacle avoidance. In this figure, the civilian vessel corresponds to the OMT vessel described in the text ([Švec et al., 2013](#)).

6.4.1. Experiment 4—Results

Fig. 19a depicts the first portion of the experiment, where the USV14 approached the first and the second approach goal while

avoiding static obstacles on its way. A maximum speed of 2 m/s was set for the global planner and the vehicle, with the exception of COLREGs crossing situations. Similar to the

“Approach” and “Following” experiment, the planner ensured a collision-free, dynamically feasible global guidance using a 4D lattice-based, global trajectory planner that considered position, orientation, and speed of the vehicle during the search for the trajectory. A satisfactory approach distance of 5 m was set for each approach point. The USV14 encountered a “head-on” situation (Fig. 19b) with an OMT vessel traveling at 1.0 m/s after it reached its second approach goal. In the absence of the OMT vessel, the USV14 would directly proceed to the third approach goal in the southwest corner. Instead, it complied with COLREGs and yielded to the OMT vessel by slowing down to 0.8 m/s and slightly turning to starboard, while ensuring it did not collide with the static obstacle region. The avoidance maneuver was performed by the local trajectory planner as described in Section 4.2.3.

Finally, after the “head-on” avoidance maneuver, the USV14 resumed its task and proceeded towards the third approach goal. On its way, the USV14 encountered another OMT vessel in the “crossing from starboard” situation. Fig. 19c depicts the USV14's

avoidance maneuver with respect to the OMT vessel. This time, the OMT vessel was traveling at an increased speed of 1.2 m/s. Thus, the USV14 had to reduce its speed rapidly to 0.7 m/s once it encountered the vessel and turned sharply to the starboard to comply with COLREGs. Table 7 displays the results over five runs of the multiple COLREGs-compliant crossing experiment and the corresponding environmental conditions over those runs. The small number of BZ incursions imply that planner was able to successfully avoid the OMT while operating in a constrained waterway.

7. Conclusions

Through on-water experiments with multiple unmanned vehicles and a manned vessel, the efficacy of using a model-referenced trajectory planner to automatically generate “Approach,” “Follow,” and COLREGs-compliant crossing behaviors in a constrained waterway has been shown. The planner developed for this effort utilizes a dynamic model of the USV and its low-level controller to forward-simulate dynamically feasible trajectories and thereby help to ensure collision-free operation. The computational efficiency of the planner is improved through adaptive sampling. The experiments presented here demonstrate that the planner can be implemented in real-time on full scale USVs. It is felt that this approach to path planning and behavior generation will permit USVs to operate over a broader range of speeds and operating conditions than standard VO-based techniques, which utilize highly simplified vehicle dynamics and do not incorporate low-level control into planning. Although not presented here, a possible avenue of extending this topic is in exploring simultaneous COLREGs crossings with multiple vehicles. Such situations may lead to conflicts where a USV must breach COLREGs in its interaction of one vehicle in order to satisfy the COLREGs governing its interaction with a second vehicle. In these instances, the problem of how to most safely and effectively perform the high-level decision making and planning required must be addressed.

Table 6
Results from the single COLREGs-compliant crossing experiment over varying environmental conditions.

| Run Number | COLREGs crossing type | Max top speed (m/s) | Number of BZ incursions | Average sustained wind speed (m/s) | Average wind gust (m/s) |
|------------|-------------------------|---------------------|-------------------------|------------------------------------|-------------------------|
| 1 | Overtaking | 1.5 | 0/3 | 2.6 | 3.8 |
| 2 | Overtaking | 1.5 | 0/3 | 2.5 | 3.8 |
| 3 | Crossing from starboard | 1.5 | 0/3 | 2.8 | 4.1 |
| 4 | Crossing from starboard | 1.5 | 0/3 | 2.6 | 4.2 |
| 5 | Head-on | 1.5 | 0/3 | 3.6 | 5.3 |
| 6 | Head-on | 1.5 | 0/3 | 3.6 | 5.3 |

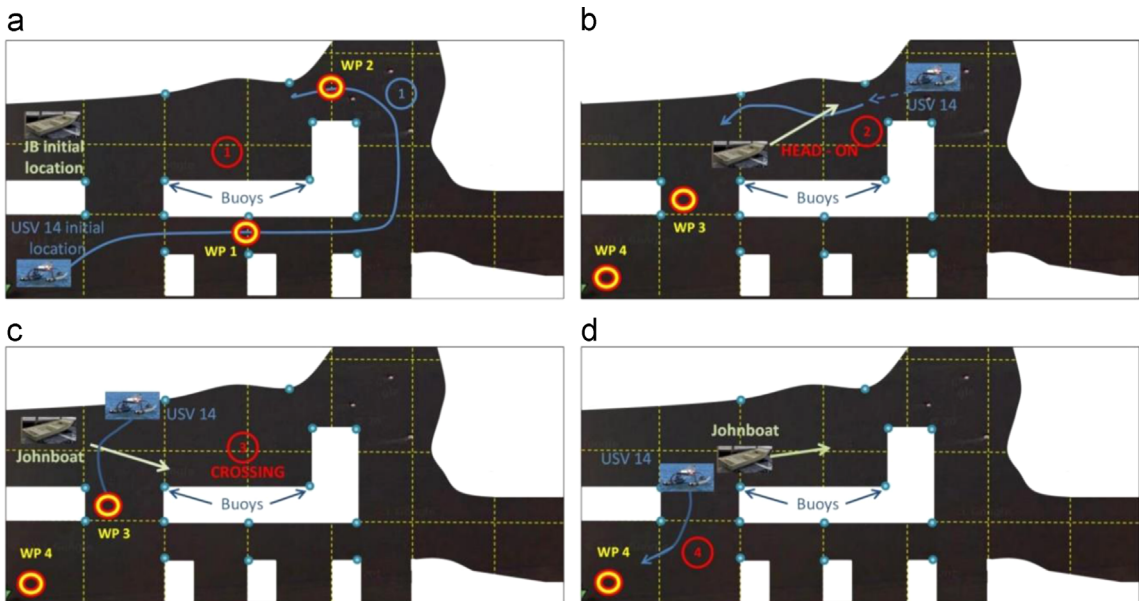


Fig. 18. Course configuration and experimental plan for multiple COLREGs crossings involving the USV14 and johnboat. The USV14 follows a trajectory according to two approach behaviors (a). Directly after that, a “head-on” COLREGs behavior is initiated (b), followed by a “crossing from starboard” behavior (c). The vehicle follows through to the final approach point (d).

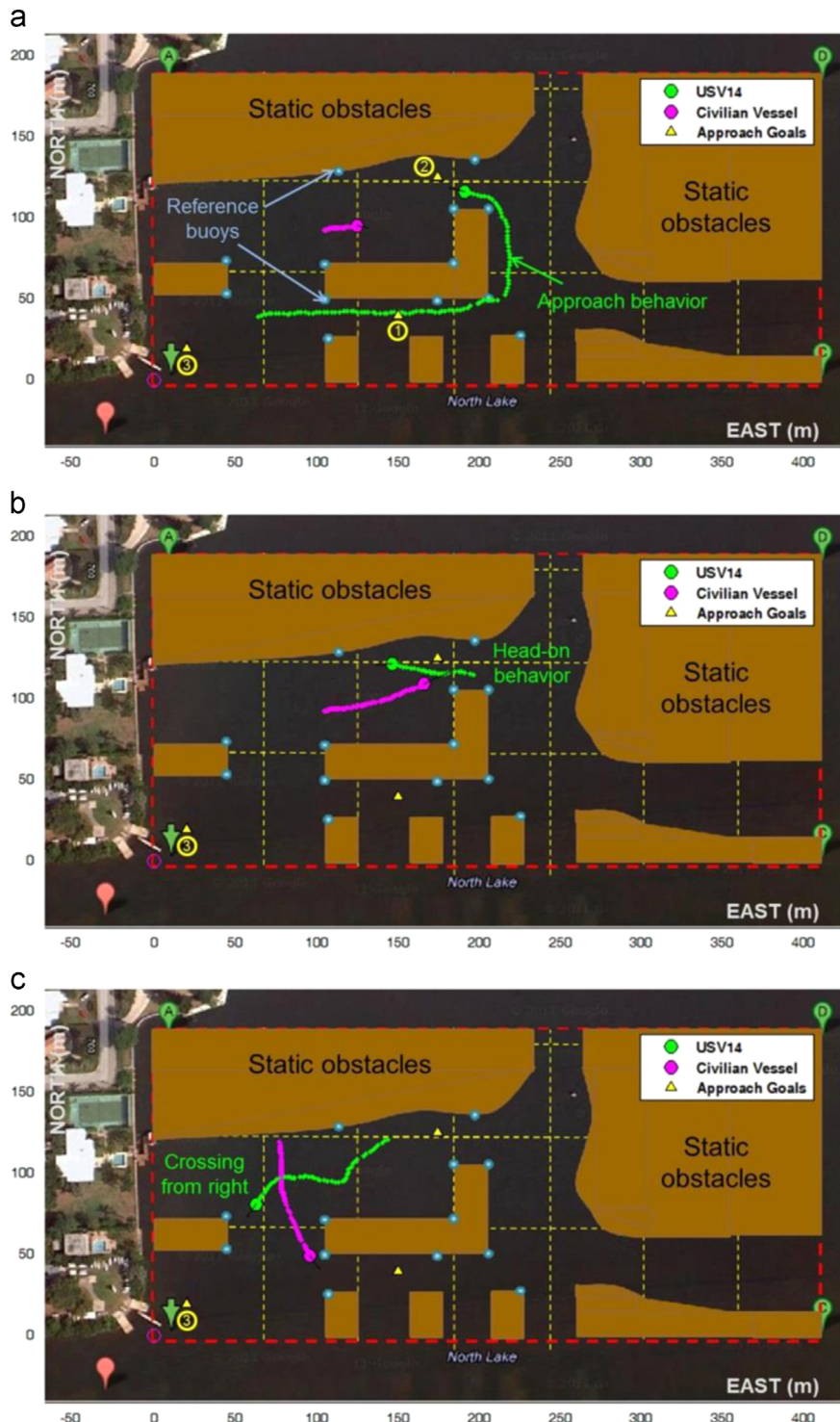


Fig. 19. Example results of a multiple COLREGs crossing experiment. In this figure, the civilian vessel corresponds to the OMT vessel described in the text.

Table 7

Results from the multiple COLREGs crossing experiments over varying environmental conditions.

| Run number | Max top speed (m/s) | Number of BZ incursions | Average sustained wind speed (m/s) | Average wind gust (m/s) |
|----------------|---------------------|-------------------------|------------------------------------|-------------------------|
| 1 | 2.0 | 0/8 | 7.0 | 9.1 |
| 2 | 2.0 | 1/8 | 6.8 | 8.9 |
| 3 ^a | 2.0 | 0/3 | 6.4 | 8.7 |
| 4 ^a | 2.0 | 1/3 | 6.8 | 8.8 |
| 5 ^a | 2.0 | 0/3 | 6.5 | 9.1 |

^a To conserve battery life, the “Approach” portion of the experiments was omitted from these runs (Fig. 18a), and the USV was started in the northeast quadrant of the map, performing the multiple COLREGs crossings (Fig. 18b-d).

Acknowledgment

This work was supported by the U.S. Office of Naval Research under Grants N000141110423 and N000141210502, managed by K. Cooper and R. Brizzolara, respectively. The first author would like to gratefully acknowledge the support of the Link Foundation Ocean Engineering & Instrumentation Ph.D. Fellowship Program.

References

- Aguiar, A.P., Hespanha, J.H., 2003. Position tracking of underactuated vehicles. In: Proceedings of the American Control Conference, Denver, CO USA.
- Aguiar, A.P., Cremean, L., & Hespanha, J.P., 2003. Position tracking for a nonlinear underactuated hovercraft: controller design and experiment results. In: Proceedings of the 42nd IEEE Conference on Decision and Control, Maui, HI USA.
- Alvarez, J., Bertaska, I., von Ellenrieder, K., 2013. Nonlinear control of an amphibious surface vehicle. In: Proceedings of the ASME Dynamic Systems and Control Conference, Palo Alto, CA.
- Ashrafiou, H., Muske, K.R., McNinch, L.C., 2010. Review of nonlinear tracking and setpoint control approaches for autonomous underactuated marine vehicles. In: Proceedings of the American Control Conference, Baltimore, MD USA.
- Ashrafiou, H., Muske, K.R., McNinch, L.C., Soltan, R.A., 2008. Sliding-Mode Tracking Control of Surface Vessels. *IEEE Trans. Ind. Electron.* 55 (11), 4004–4011.
- Bareiss, D., van den Berg, J., 2013. Reciprocal collision avoidance for robots with linear dynamics using LQR-obstacles. In: Proceedings of the IEEE International Conference on Robotics and Automation, Karlsruhe, Germany.
- Benjamin, M.R., Leonard, J.J., Curcio, J.A., Newman, P.A., 2006. Protocol-based COLREGs collision avoidance navigation between unmanned surface craft. *J. Field Robot.* 23, 5.
- Bertaska, I.R., Alvarez, J., Sinisterra, A.J., von Ellenrieder, K., Dhanak, M., Shah, B., Švec, P., Gupta, S.K., 2013. Experimental evaluation of approach behavior for autonomous surface vehicles. In: Proceedings of the ASME Dynamic Systems and Control Conference, Palo Alto, California.
- Bibuli, M., Caccia, M., Lapierre, L., Bruzzone, G., 2012. Guidance of unmanned surface vehicles: experiments in vehicle following. *IEEE Robot. Autom. Mag.* 19 (3), 92–102.
- Bingham, B., Walls, J., Eustice, R., 2011. Development for a flexible command and control software architecture for robotic marine applications. *Mar. Technol. Soc. J.* 3 (45), 26–36.
- Campbell, S., Naeem, W., Irwin, G.W., 2012. A review on improving the autonomy of unmanned surface vehicles through intelligent collision avoidance manoeuvres. *Ann. Rev. Control.* 36, 267–283.
- Commandant, U.C.G., 1999. International regulations for prevention of collisions at sea, 1972 (72 COLREGS). US Department of Transportation, US Coast Guard, COMMANDANT INSTRUCTION M 16672.
- Do, K.D., 2010. Practical control of underactuated ships. *Ocean Eng.* 37, 1111–1119.
- Do, K.D., Pan, J., 2003. Global tracking control of underactuated ships with off-diagonal terms. In: Proceedings of the 42nd IEEE Conference on Decision and Control, Maui, Hawaii, USA.
- Fiorini, P., Shiller, Z., 1998. Motion planning in dynamic environments using velocity obstacles. *Int. J. Robot. Res.* 17 (7), 760–772.
- Fossen, T.I., 1994. Guidance and Control of Marine Vehicles, 199. Wiley, New York.
- Fossen, T.I., 2002. Marine Control Systems. Tapir Trykkeri, Trondheim, Norway.
- Fox, D., Burgard, W., Thrun, S., 1997. The dynamic window approach to collision avoidance. *IEEE Robot. Autom. Mag.* 4 (1), 23–33.
- Frachard, T., Asama, H., 2004. Inevitable collision states—a step towards safer robots? *Adv. Robot.* 18 (10), 1001–1024.
- Gadre, A.S., Du, S., Stilwell, D.J., 2012. A Topological Map Based Approach to Long Range Operation of An Unmanned Surface Vehicle. In: Proceedings of the American Control Conference, Montreal, QC Canada.
- Gat, E., 1993. On the role of stored internal state in the control of autonomous mobile robots. *AI Mag.* 14 (1), 64.
- Gat, E., 1998. On three-layer architectures. *Artif. Intell. Mob. Robots* 195, 210.
- Hart, P.E., Nilsson, N.J., Raphael, B., 1968. A formal basis for the heuristic determination of minimum cost paths. *IEEE Trans. Syst. Sci. Cybern.* 4 (2), 100–107.
- Howard, T.M., Green, C.J., Kelly, A., Ferguson, D., 2008. State space sampling of feasible motions for high-performance mobile robot navigation in complex environments. *J. Field Robot.* 25 (6–7), 325–345.
- Khalil, H.K., 2002. Nonlinear systems. Prentice Hall, Upper Saddle River, NJ.
- Klinger, W., Bertaska, I.R., von Ellenrieder, K.D., 2015. Control of an unmanned surface vehicle with uncertain displacement and drag. *IEEE Journal of Oceanic Engineering*, Submitted for publication, under review.
- Klinger, W., Bertaska, I.R., von Ellenrieder, K., Alvarez, J., 2013. Controller design challenges for waterjet propelled unmanned surface vehicles with uncertain drag and mass properties. *MTS/IEEE Oceans*, San Diego, CA USA.
- Kuwata, Y., Wolf, M., Zarzhitsky, D., Huntsberger, T., 2014. Safe maritime autonomous navigation with COLREGs, using velocity obstacles. *IEEE J. Ocean. Eng.* 39 (1), 110–119, doi: 10.1109.
- Lee, S., Kwon, K., Joh, J., 2004. A fuzzy logic for autonomous navigation of marine vehicles satisfying COLREG guidelines. *Int. J. Control. Autom. Syst.* 2, 171–181.
- Liao, Y., Pang, Y., Wan, L., 2010. Combined Speed and Yaw Control of Underactuated. In: Proceedings of the 2nd International Asia Conference on Informatics in Control, Automation and Robotics, Wuhan, China.
- Likhachev, M., Ferguson, D.I., Gordon, G.J., Stentz, A., Thrun, S., 2005. Anytime Dynamic A*: An Anytime, Replanning Algorithm. In: Proceedings of the International Conference on Automated Planning and Scheduling (ICAPS), pp. 262–270.
- Mahini, F., Ashrafiou, H., 2012. Autonomous Surface Vessel Target Tracking Experiments in Simulated Rough Sea Conditions. In: Proceedings of the ASME Dynamic Systems and Control Conference, Ft. Lauderdale, FL USA.
- Marquardt, J.G., Alvarez, J., von Ellenrieder, K.D., 2014. Characterization and System Identification of an Unmanned Amphibious Tracked Vehicle. *IEEE J. Ocean. Eng.* 39 (4), 641–661.
- Pettersen, K.Y., Egeland, O., 1996. Exponential Stabilization of an Underactuated Surface Vessel. In: Proceedings of the Conference on Decision and Control, Kobe, Japan.
- Pivtoraiko, M., Knepper, R.A., Kelly, A., 2009. Differentially constrained mobile robot motion planning in state lattices. *J. Field Robot.* 26 (3), 308–333.
- Ridao, P., Batlle, J., Amat, J., Roberts, G.N., 1999. Recent trends in control architectures for autonomous underwater vehicles. *Int. J. Syst. Sci.* 30 (9), 1033–1056.
- Sgorbissa, A., Zaccaria, R., 2012. Planning and obstacle avoidance in mobile robotics. *Robot. Auton. Syst.* 60 (4), 628–638.
- Shah, B., Švec, P., Gupta, S.K., 2015. Resolution adaptive risk-aware trajectory planning for autonomous surface vehicles operating in congested civilian traffic. *Autonom. Robots*, Submitted for publication, under review.
- Slotine, J.-E., Li, W., 1991. Applied Nonlinear Control. Prentice Hall, Englewood Cliffs, NJ USA.
- Sonnenburg, C.R., Woolsey, A.C., 2013. Modeling, identification, and control of an unmanned surface vehicle. *J. Field Robot.* 30 (3), 1–28.
- Stachniss, C., Burgard, W., 2002. An integrated approach to goal-directed obstacle avoidance under dynamic constraints for dynamic environments. In: Proceedings of the IEEE/RSJ International Conference on Intelligent Robots and Systems 1, pp. 508–513.
- Stilwell, D.J., Gadre, A.S., Kurdila, A.J., 2011. A receding horizon approach to generating dynamically feasible plans for vehicles that operate over large areas. In: Proceedings of the IEEE/RSJ International Conference on Intelligent Robots and Systems, San Francisco, CA USA.
- Švec, P., Gupta, S.K., 2012. Automated synthesis of action selection policies for unmanned vehicles operating in adverse environments. *Auton. Robots* 32 (2), 149–164.
- Švec, P., Shah, B.C., Bertaska, I.R., Alvarez, J., Sinisterra, A.J., von Ellenrieder, K., Dhanak, M., Gupta, S.K., 2013. Dynamics-aware target following for an autonomous surface vehicle operating under COLREGs in civilian traffic. In: Proceedings of the IEEE/RSJ International Conference on Intelligent Robots and Systems, Tokyo, Japan.
- Švec, P., Shah, B.C., Bertaska, I.R., Klinger, W., Sinisterra, A.J., von Ellenrieder, K., Dhanak, M., Gupta, S.K., 2014a. Adaptive sampling based COLREGs-compliant obstacle avoidance for autonomous surface vehicles. In: Proceedings of the IEEE International Conference on Robotics and Automation, Hong Kong, China.
- Švec, P., Shah, B.C., Bertaska, I.R., Klinger, W., Sinisterra, A.J., von Ellenrieder, K., Dhanak, M., Gupta, S.K., 2014b. Trajectory planning with adaptive control primitives for autonomous surface vehicles operating in congested civilian traffic. In: Proceedings of the IEEE/RSJ International Conference on Intelligent Robots and Systems, Chicago, IL USA.
- Švec, P., Thakur, A., Raboin, E., Shah, B.C., Gupta, S.K., 2014c. Target following with motion prediction for unmanned surface vehicle operating in cluttered environments. *Auton. Robots* 36 (4), 383–405.
- Thukar, A., Švec, P., Gupta, S.K., 2012. GPU Based Generation of State Transition Models Using Simulations for Unmanned Sea Surface Vehicle Trajectory Planning. *Robot. Auton. Syst.* 60 (12), 1457–1471.
- van den Berg, J., Snape, J., Guy, S.J., Manocha, D., 2011. Reciprocal collision avoidance with acceleration-velocity obstacles. In: Proceedings of the International Conference on Robotics and Automation, Shanghai, China.
- van den Berg, J., Wilkie, D., Guy, S., Niethammer, M., Manocha, D., 2012. LGQ-obstacles: feedback control with collision avoidance for mobile robots with motion and sensing uncertainty. In: Proceedings of the IEEE International Conference on Robotics and Automation, Saint Paul, MN USA.
- Wilkie, D., van den Berg, J., Manocha, D., 2009. Generalized Velocity Obstacles. In: Proceedings of the IEEE/RSJ International Conference on Intelligent Robots and Systems, St. Louis, MO USA.